JOURNAL OF MATERIALS SCIENCE 19 (1984) 2013–2038

Stress–orientation–strain relationships in non-crystalline polymers

Part 2 *The two-component model developed and applied to rubber-like deformation*

D. J. BROWN, A. H. WINDLE
Department of Metallurgy and Materials Science, Unversity of Cambridge, Cambridge, UK

The approach to non-crystalline polymer deformation set out in Part 1 [1], involving the resolution of deformation into orientational and non-orientational components, is employed as the foundation of a simple deformation model applicable to the rubbery state. The analysis is performed with reference to an assemblage of mobile orienting units of idealized ellipsoidal shape, free to undergo orientational and extensional motion but subject to constraint arising from both intramolecular and intermolecular sources. Stress–strain–orientation relationships are calculated and compared to alternative theories and to experiment, with particular reference to poly(methyl methacrylate) and poly(ethylene terephthalate).

1. A model for rubber-like deformation

We now employ the general approach established in Part 1 [1] as the foundation for a more detailed deformation model. The chief objective in doing so will be to examine the utility of the basic two-component philosophy set out above. To that end, it is important to keep the model as general and simple as possible at this stage. A central aim in taking this unconventional approach is to resolve difficulties encountered by conventional models in dealing with some aspects of stress–orientation–strain behaviour. Of course, success in areas of difficulty is not in itself sufficient justification for a new strategy: the strategy has also to offer at least as satisfactory a description of standard rubber-like behaviour as do established approaches.

The orientational deformation mode is conceptually the easier to deal with. We neglect, initially, the effect of specific interactions between chain segments, and develop an energy argument in terms of the work done by an applied stress as a consequence of "orientational" deformation.

1.1. The orientational mode: a first approximation

Consider a solid cylindrical body of height H and cross-sectional area A, containing "orienting units" such as that in Fig. 1. Let a compressive stress σ act radially on the curved surface, but not on the ends. The deviatoric component of such a stress is the same as for uniaxial tension: since we may assume that deformation (at constant volume) is dependent only on the deviatoric and not on the hydrostatic component of the stress tensor, we can take the deformation behaviour to be equivalent to that of uniaxial tension.

If we allow an orienting unit to undergo a small rotation $d\phi$ about its centre (Fig. 2), the stress does work given by:

$$\text{force} \times \text{distance through which force acts}$$

$$= (\text{force on a "slice" of height } 2l\cos\phi) \times dR$$

$$= \sigma 2\pi R\, 2l\cos\phi \times dR$$

(neglecting the possibility of the section intersecting either end of the unit – which implies, in effect, very long units). Consideration of a cross-section through the body (Fig. 3) shows that the unit at angle ϕ, together with its share of the unoccupied volume, contributes an area

$$A_\phi = \pi a^2/(\alpha\cos\phi) \quad (1)$$

0022–2461/84 $03.00 + .12

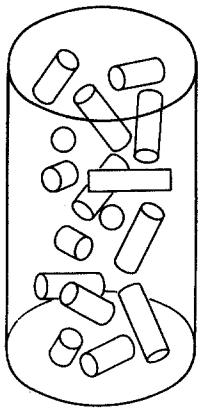

Figure 1 Cylindrical assemblage of "orienting units".

to the cross-section, where α, the packing density, is less than 1 and assumed constant. The change in area dA due to the small rotation is therefore

$$dA = (\pi a^2/\alpha) \sec\phi \tan\phi \, d\phi \qquad (2)$$

But

$$dA = 2\pi R dR$$

so

$$\text{work done} = \sigma v \tan\phi \, d\phi$$

where v, the volume per unit, is simply $2\pi a^2 l/\alpha$. Thus the total work done in rotating from $\phi = \phi_1$ to $\phi = 0$ is given by

$$W = \sigma v \int \tan\phi d\phi \qquad \text{limits } 0, \phi_1$$

$$= -\sigma v \log\cos\phi_1 \qquad (3)$$

We can therefore assign an energy $U = U_0 + W$ to a unit at angle ϕ (where U_0 is energy associated with a unit at $\phi = 0$).

Having now a relationship between ϕ and

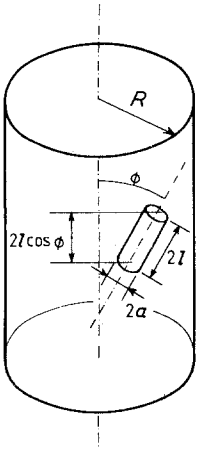

Figure 2 Detail of one "orienting unit", defining terms used in the text.

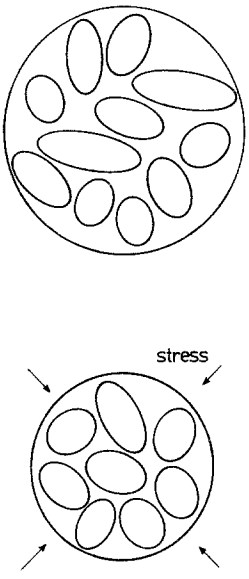

Figure 3 Cross-section or "sampling plane" through the assemblage.

energy, the next step is to determine the equilibrium orientational distribution of units in a stress field σ at a temperature T.

The solid angle at ϕ to some axis is proportional to $\sin\phi$ or, using the language of energy states, there are more states available at high ϕ, i.e.

$$\text{Degeneracy } D(\phi) \sim \sin\phi$$

Under stress the simplest assumption we can make is of a "Boltzmann" form, so that the probability of a unit being at an angle in the range ϕ to $\phi + d\phi$ is given by:

$$p(\phi)d\phi \sim D(\phi) \exp(-U/kT) d\phi \qquad (4)$$

This probability distribution corresponds to the distribution function in ϕ, from which the usual spherical harmonics may be derived. However, if we were to cut a section horizontally through the assemblage, the probability $p'(\phi)$ of actually finding (cutting through) such a unit would be different. We would be less likely to find one at high ϕ (near $\pi/2$) because the component of its length perpendicular to our cutting plane is proportional to $\cos\phi$. Hence

$$p'(\phi) \, d\phi \sim \sin\phi \cos\phi \exp(-U/kT) \, d\phi \qquad (5)$$

However,

$$\exp(-U/kT) = \exp(-U_0/kT) \exp(q \log\cos\phi)$$

$$= \exp(-U_0/kT)(\cos^q\phi)$$

introducing the dimensionless variable

$$q = \sigma v/kT \quad (6)$$

Hence

$$p'(\phi)\,d\phi = \text{constant} \times \sin\phi \cos\phi \cos^q\phi\, d\phi \quad (7)$$

The total cross-sectional area of our body will be

$$A = \frac{N\int A_\phi p'(\phi)d\phi}{\int p'(\phi)d\phi} \quad \text{(limits } 0, \pi/2) \quad (8)$$

(where N = number of units cutting cross-section, and A_ϕ = area of intercept associated with a unit at angle ϕ, as defined by Equation 1. Equation 8 can be written as:

$$A = \frac{N\pi a^2}{\alpha} \frac{\int \sec\phi \cos\phi \cos^q\phi\, d(\cos\phi)}{\int \cos\phi \cos^q\phi\, d(\cos\phi)}$$

$$= \frac{N\pi a^2}{\alpha} \times \frac{(q+2)}{(q+1)} \quad (9)$$

At zero stress ($q = 0$), let $A = A_0$, $H = H_0$, and $N = N_0$. Clearly

$$A_0 = 2N_0\pi a^2/\alpha \quad (10)$$

so the extension ratio λ is given (assuming constant volume, i.e., constant α) by:

$$\lambda = H/H_0 = A_0/A$$

$$= 2\frac{N_0}{N} \times \frac{(q+1)}{(q+2)} \quad (11)$$

where the orientational component λ_0 of the extension ratio is simply

$$\lambda_0 = 2(q+1)/(q+2)$$

If the orientational process were the sole deformation mode, N would be constant ($N = N_0$) and the maximum strain 100% ($\lambda = 2$). The corresponding plot of q against λ_0 is shown in Fig. 4; this is effectively a true stress–extension ratio curve since for constant temperature $q \propto \sigma$. Relationships between stress and orientation also follow from this development: they are considered below.

1.2. More realistic units

The argument above is valid so long as we forget that cylinders have ends. We have assumed that the "intercept area" of a unit with the sampling plane will vary as $(1/\cos\phi)$, which clearly approaches infinity as ϕ approaches $\pi/2$. For a finite-length cylindrical unit this intercept area should tend instead to some finite value at $\phi = \pi/2$. The shorter the unit, the lower the angle ϕ at which the ends begin to matter – and for a real material a reasonable "unit" may be so short and squat that the "long cylinder" assumption ($l \gg a$) must be rejected.

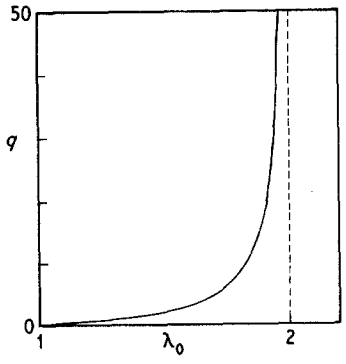

Figure 4 True stress parameter q against orientational component of extension ratio λ_0.

Short fat cylinders are not particularly pleasant to deal with, because their surfaces are not mathematically smooth and continuous. A more easily handled – and conceptually nicer – shape is provided by a prolate ellipsoid of revolution (a rugby ball!). The geometry of such a shape is a little tedious, so it is in Appendix I, where an argument similar to the above leads to:

$$\frac{A_0}{A} = \frac{N_0}{N} \times \frac{2}{\left[1 + \frac{m^2}{e}\ln\left(\frac{1+e}{m}\right)\right]} \frac{1}{m} \frac{\int \sec^{q+2}\psi d\psi}{\int \sec^{q+3}\psi d\psi} \quad (12)$$

(with limits of integration 0, arc cos $(m^{1/2})$. Here e is the eccentricity of the ellipsoid and, to simplify the algebra, $m^2 = (1 - e^2)$: the "aspect ratio" of the ellipsoid is simply $1/m$.

According to Equation 12, A_0/A (i.e. λ_0) varies with q as shown in Fig. 5. The maximum orientational strain is clearly zero if the aspect ratio of the ellipsoid is 1 (a sphere) and approaches 100%, corresponding to our simpler argument above, as the aspect ratio tends to infinity (Fig. 6).

1.3. The extensional component: a simple calculation

The argument above would hold for any liquid composed of molecules of anisotropic shape.

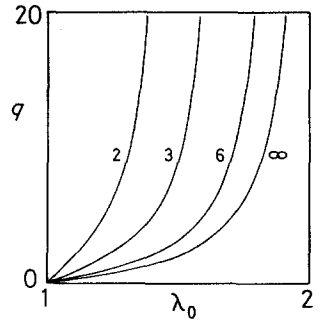

Figure 5 True stress parameter q against λ_0 for ellipsoidal units (number denotes ellipsoid aspect ratio).

However, the ability of the molecules to flow past one another and the overall dimensional changes thus possible would completely swamp the strain associated with their orientation induced by the stress field (although the orientation itself would be manifest as flow birefringence). In envisaging orienting units which are more-or-less flexibly joined into chains, as in a polymer, the "flow" – the extensional component of deformation – is limited. We are not considering here the possibility of changes in the relative positions of the centres of gravity of the complete macromolecules, as might occur during the viscous flow of a melt.

To model the non-orientational mode of deformation we allow the units to slide past one another so as to reduce the average number intercepting a cross-section through the cylindrical assemblage. A similar argument to that of the orientational mode can be employed, in terms of the work done by an applied stress.

As a first approximation, suppose we build up the assemblage unit by unit. Let there be two ways (neglecting orientational states) in which each successive unit may be added, as indicated in Fig. 7: either:

(a) alongside its predecessor, in the same "layer"; or

(b) in an adjacent "layer" to, but above, its predecessor.

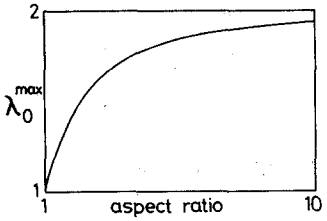

Figure 6 Maximum rotational strain λ_0^{max} as a function of unit aspect ratio.

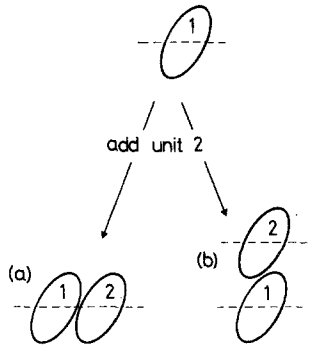

Figure 7 Extensional deformation mode. Unit 2 may be added to the assemblage in one of two ways with respect to unit 1: (a) "alongside" (b) in a different "layer".

Suppose that the probabilities of these conditions are P_a and P_b respectively. In the absence of stress, let $(P_a/P_b) = (P_a/P_b)_0$, and the number of units intersecting an average cross-section be N_0.

If we now impose an applied stress then, neglecting rotation, the new number N intersecting such a cross-section will be given by

$$\frac{N}{N_0} = \frac{(P_a/P_b)}{(P_a/P_b)_0} \tag{13}$$

If one unit changes from state (a) to state (b) we will have an average macroscopic dimensional change in the body, such that the applied stress σ will do work (Fig. 8)

$$W = v\sigma = qkT \tag{14}$$

where as above, v is the volume per mobile unit. Again the simplest assumption we can make is of a "Boltzmann" form, so that we write:

$$\frac{P_b}{P_a} = \frac{1}{K}\exp(W/kT) = \frac{1}{K}\exp(q)$$

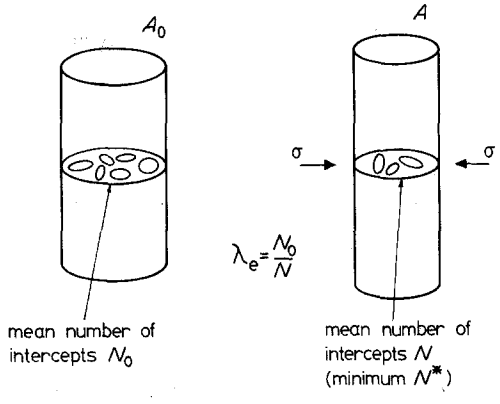

Figure 8 Work associated with dimensional change due to extensional deformation.

or

$$\frac{(P_a/P_b)}{(P_a/P_b)_0} = \exp(-q) \qquad (15)$$

If all units had this choice between states, we should now obtain

$$(N/N_0) \sim \exp(-q) \qquad (16)$$

However, such a model would not be very appropriate to a real solid, in which molecular segments are subject to constraints on their freedom of movement due to their neighbours – chemical cross-links, mechanical entanglements, steric hindrance, and particularly in a polymer the effect of neighbouring portions of the same main chain.

To model this constraint in detail would be most difficult, and numerous workers have given attention to the problem. We therefore introduce a simplification. A mobile unit will, "on average", fall somewhere between the two extremes of complete freedom of extensional movement on the one hand, and complete restraint of extensional motion on the other. Let the mean constraint on extensional deformation be $1/K$, so that $0 < 1/K < 1$ (it is a computational convenience to use the reciprocal, since we then deal with a parameter greater than 1). We now replace the "distribution of fractional constraint", with mean value $1/K$, by dividing the N_0 units cutting a typical plane through the assemblage into two categories. Let one set, containing N^* units, be completely constrained, and the remaining $(N_0 - N^*)$ units be fully free to undergo extensional deformation, with

$$N^*/N_0 = 1/K$$

In this simplified picture, the first set will be confined in effect to state (a) i.e., unable to leave the selected cross-section. Fig. 9 depicts the situation in terms of the three-dimensional chain: we visualize the chain segment shown as being "pulled" in a direction normal to the sampling plane so that the number of "intersections" is reduced to a minimum of one. Equation 16 can now be modified to give

$$N = (N_0 - N^*)\exp(-q) + N^* \qquad (17)$$

which after a little rearrangement produces

$$(N/N_0) = (1/K) + (1 - 1/K)\exp(-q) \qquad (18)$$

with

$$K = N_0/N^* \qquad (19)$$

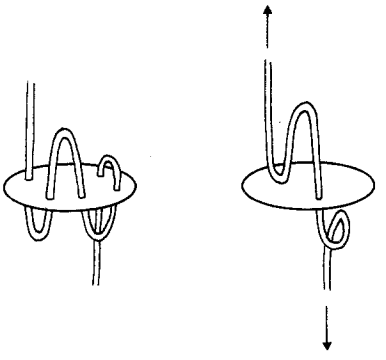

Figure 9 A schematic representation of extensional deformation. The number of intercepts with the sampling plane is reduced to a lower limit (here 1) as the chain segment is "pulled" normal to the plane.

The extensional component λ_e of the extension ratio is then the reciprocal of this expression, (N_0/N). The relationship is shown graphically in Fig. 10 for the case $K = 3$.

Physically, the "average constraint" $1/K$ represents the resultant effect on extensional deformation of linkages between units along the polymer chain, chemical cross-linking, mechanical entanglements and steric hindrances.

1.4. A refinement of the extensional deformation component

Consider again the two states (a), (b). Treating these as energy states, let the number of available sites in these states at zero stress be in a ratio M. Since at zero stress we can take the energies of the two states to be equal, their occupancies, denoted n_1^0, n_2^0, will be in the same ratio M. At a finite stress, state (b), "absent from the sampling plane", will be favoured, and again assuming

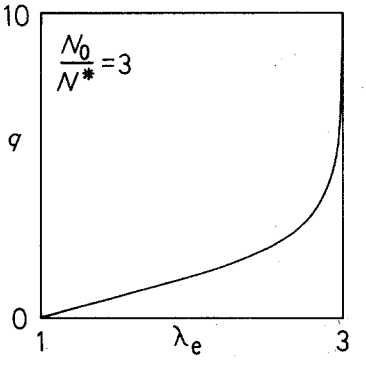

Figure 10 True stress parameter q against translational component of extension ratio λ_e for the case $K = 3$ (i.e., 1/3 of the intercepts on each cross-section are fixed and cannot be expelled by stress).

Boltzmann statistics we write

$$n_1/n_2 = M \exp(-q) \tag{20}$$

where n_1, n_2 are the occupancies at finite stress. There are $(N_0 - N^*)$ units per sampling plane which are able to distribute themselves between these states, so that

$$n_1^0 = N_0 - N^* \tag{21}$$

and therefore

$$\frac{N_0 - N^*}{n_2^0} = M \tag{22}$$

Similarly, at finite stress,

$$n_1 = N - N^* \tag{23}$$

But since the total number of units $(n_1 + n_2)$ in our hypothetical system must be constant,

$$N_0 - N^* + n_2^0 = N - N^* + n_2 \tag{24}$$

Using Equation 22 we then have

$$\begin{aligned} n_2 &= (N_0 - N^*) - (N - N^*) + (N_0 - N^*)/M \\ &= N_0(1 + 1/M) - N - N^*/M. \end{aligned} \tag{25}$$

Substituting for n_1 and n_2 in Equation 20,

$$(N - N^*) = (MN_0 + N_0 - MN - N^*) \exp(-q) \tag{26}$$

and rearranging,

$$\begin{aligned} &N[1 + M \exp(-q)] \\ &\quad = N_0(1 + M) \exp(-q) + N^*[1 - \exp(-q)] \\ \lambda_e &= \frac{N_0}{N} \\ &= \frac{1 + M \exp(-q)}{(1 + M) \exp(-q) + (N^*/N_0)[1 - \exp(-q)]} \end{aligned} \tag{27}$$

which is our expression for the extensional component λ_e of the extension ratio.

It will presumably be reasonable to use a model where there are more available sites "absent from" the sampling plane than "present", so that M will be less than 1. The case $M \simeq 0$ (very many more "absent" states) is equivalent to the simpler argument above. The two cases $M = 0$, $M = 1$ are plotted in Fig. 11: given that a reasonable choice for M would be small, it is clear that the more rigorous model makes in practice only a slight difference to the stress–strain relationship, at least in tension. It will be convenient for most purposes, therefore, to take $M = 0$ and use the simpler model.

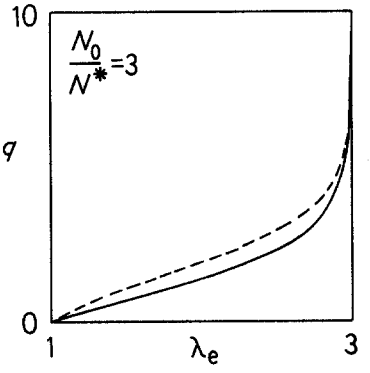

Figure 11 Effect of modified expression for λ_e. Solid line: $M = 0$ (as previous figure); dashed line: $M = 1$.

1.5. Resultant stress–strain behaviour

We have now derived expressions for each of the two components of strain, the orientational and the extensional. The overall extension ratio λ will be given by the product

$$\lambda(q) = \lambda_0 \lambda_e \tag{28}$$

with the explicit equations for λ_0 and λ_e given by Equations 12 and 27. Since it is conventional to represent stress–strain behaviour in terms of either "nominal" or "true" parameters, we make use of the following relationships:

Nominal strain $\epsilon_n = \lambda - 1$

True strain $\epsilon_t = \ln(1 + \epsilon_n) = \ln \lambda$

Nominal stress $\sigma_n = \sigma/\lambda$

and hence define a "nominal stress parameter" Q such that

$$Q = q/\lambda.$$

1.6. Calculation of orientation parameters

Values of the spherical harmonic parameters $\langle P_{2n} \rangle$ may be calculated in an analogous way to the calculation of λ_0. They will vary only with the orientational component of the deformation, since $\langle \cos^{2n}\phi \rangle$ is a function of λ_0 but not of λ_e. The shape of the plot will of course change with λ_e if the orientation parameter is plotted against some parameter other than the "true stress parameter" q, since λ_e does affect the transformation from q to other measures of stress or strain. From Equation 4 the probability of a "unit" lying between ϕ and $\phi + d\phi$ is

$$\begin{aligned} p(\phi)d\phi &\sim D(\phi) \exp(-U/kT)d\phi \\ &\sim \text{constant} \times \sin\phi \cos^q\phi \, d\phi \end{aligned}$$

Average values of $\cos^{2n}\phi$ will then be given by

$$\langle\cos^{2n}\phi\rangle = \frac{\int_0^{\pi/2}\cos^{2n}\phi p(\phi)\mathrm{d}\phi}{\int_0^{\pi/2}p(\phi)\mathrm{d}\phi} \quad (29)$$

For $n = 1$ we obtain

$$\langle\cos^2\phi\rangle = \frac{\int_0^1\cos^{q+2}\phi\,\mathrm{d}(\cos\phi)}{\int_0^1\cos^q\phi\,\mathrm{d}(\cos\phi)} \quad (30)$$

$$= \frac{q+1}{q+3} \quad (31)$$

and similarly for general n,

$$\langle\cos^{2n}\phi\rangle = \frac{q+1}{q+2n+1} \quad (32)$$

From the definitions of $P_{2n}(\cos\phi)$ we then obtain

$$\langle P_2(\cos\phi)\rangle = \frac{1}{2}\left(3\frac{q+1}{q+3}-1\right) \quad (33)$$

$$\langle P_4(\cos\phi)\rangle = \frac{1}{8}\left(35\frac{q+1}{q+5}-30\frac{q+1}{q+3}+3\right) \text{ etc.} \quad (34)$$

The calculation of P_{2n} values can be extended to our ellipsoidal units by a similar method to that employed for λ_0: the detailed calculation is given in Appendix I.

2. Behaviour of the model

With the derivation of the $\langle P_{2n}\rangle$ terms in the orientation distribution function, we now have the necessary equations to describe the stress–orientation–strain relationship for the system. In the limiting case of infinite aspect ratio (Equation 11) the stress–strain curve is described by:

$$\lambda(q) = 2\frac{(q+1)}{(q+2)}\times\frac{1}{[1/K+(1-1/K)\exp(-q)]} \quad (35)$$

True stress (σ_t) is proportional to q (Equation 6), while nominal stress (σ_n) is just σ_t/λ. As will be illustrated below, the introduction of finite aspect ratios does not greatly affect the overall shape of the curve.

The orientation–true stress relationship, given for infinite aspect ratio by Equations 33, 34, etc., is independent of the constraint parameter K, though the latter does affect the orientation–nominal stress and orientation–strain plots. Such curves are easily determined numerically, but cannot be represented simply by an analytical expression since Equation 35 is transcendental.

To plot typical stress–orientation–strain relationships we now need to select appropriate values for the unit aspect ratio and the constraint parameter K, i.e. the ratio N_0/N^*. The selection is best made in the light of information obtainable from experiment or from molecular considerations.

The first item of information of which we can make use is the maximum strain of the system. The model will predict a maximum extension ratio given by $\lambda_0^{\max}K$, where the maximum orientational component $\lambda_0^{\max}$ will be 2 for the "first approximation" model and somewhat less, as calculated in Appendix I, for units with a finite aspect ratio. Now if we consider typical nominal stress–strain curves for real polymers in the rubbery state, and extrapolate the high-strain portion roughly, the plot will tend towards a limiting extension ratio of typically 6 to 9 for natural rubber, and rather less for other polymers. If the model is satisfactory at low to moderate strains we might expect the curve to turn up towards an asymptote rather more abruptly, and at a rather lower strain, than experiment indicates. This is because the model as it stands makes no allowance for the "pulling-out" of entanglements, possible chain scission, and other effects which may be associated with high strains and hence very high stresses. In addition, our assumption of a fixed unit aspect ratio, and our use of the constraint concept as something which can be expressed as a fixed fraction of totally constrained units, means that we have nothing strictly analogous to the effect of a distribution of chain contour lengths. It is that distribution which has been associated with the failure of conventional models to deal adequately with the high strain end of the stress–strain curves of rubbers. Chains of low contour length would tend to reach maximum extensibility earlier than those of higher contour length, and this would make the high-strain phenomena appear less abruptly than for a set of chains of uniform length: similarly in the two-mode model we may expect effects at high strain to come into play more sharply than would be seen in a real polymer. In the light of the foregoing, it would be most sensible to choose our parameters such that the predicted maximum strain is similar to, or perhaps rather less than, the limiting strain which we should expect by

extrapolation of real nominal stress–strain curves.

The second item of information which would be of value concerns the aspect ratio of the "orienting unit". We consider the problem in more detail below, but for our present purposes a rough idea will do. The statistical random link of conventional rubber elasticity might be a lower bound on the unit size. It would typically correspond to several monomer units, though exact sizes are uncertain: this might suggest a fairly slender ellipsoidal unit, though the inclusion of free volume around the chain would reduce the aspect ratio. For some polymers a certain amount of conformational information is available: for example, a consideration of the structure of PMMA using WAXS [2, 3] indicates that the underlying conformation (near all-*trans*) is typically preserved over about 16–20 backbone bonds or 8–10 repeat units*. While we can make use of conformational information in assessing the two-mode model, it is important to note that the model does not rest upon any detailed conformational assumptions.

These considerations alone will not allow detailed specification of the unit size and aspect ratio for a given polymer, but they nevertheless offer some general guidance and underline the importance of comparing any proposed unit with the macromolecular chain. We select an aspect ratio of 3 as perhaps "typical". The choice is still rather arbitrary, but the model is relatively insensitive to the parameter with respect to the shape of the stress–strain and orientation–strain curves; the orientational behaviour to be considered below will provide more concrete information.

To obtain a reasonable maximum strain we have to select K. A value of 3 for K would give a maximum extension ratio of 6 with units of infinite aspect ratio (needles) and rather less with more realistic units. This means, if we think back to the original discussion of the constraint concept, that we are assuming 33% constraint, on average, on an orienting unit. It would be unwise to try and justify the 33% with precision on the basis of cross-linking, inter-unit bond and steric hindrance, but a figure of a few tens of per cent is, at least, plausible, and consistent with experimental estimates of maximum extension ratio.

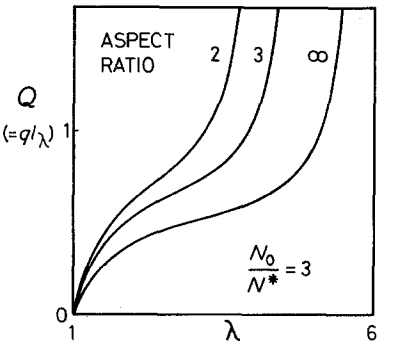

Figure 12 Effect of unit aspect ratio on the nominal stress–strain curve ($K = 3$). λ = extension ratio, Q is proportional to nominal stress. Number denotes aspect ratio.

Fig. 12 shows the predicted stress–strain curve for $K = 3$ and aspect ratios ranging from 2, a squat ellipsoid, to infinity, the limiting case of "long thin needles" described by Equation 35. The overall shape of the curve, particularly for the finite aspect ratios, is typical of those observed for polymers in the rubbery regime. Fig. 13 shows a similar set of curves, this time with a fixed aspect ratio of 3 and K varying around the value of 3 suggested above. Finally, the model prediction with a parameter values suggested is compared to the Gaussian theory in Fig. 14.

2.1. Orientation development

The orientation–stress behaviour predicted by the model is shown in Fig. 15 (for the first two Legendre polynomials), again for a range of unit aspect ratio: these curves are independent of K.

The strain-optical coefficient (SNOC) is given

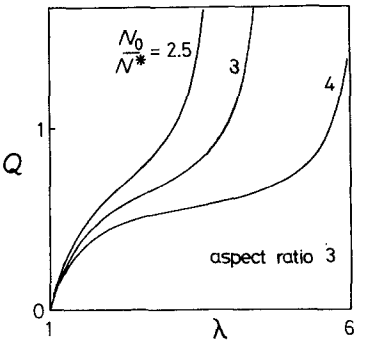

Figure 13 Effect of constraint parameter K ($= N_0/N^*$) on the nominal stress–strain curve.

*This length is actually deduced from data for syndiotactic PMMA, but we can apply it here since the scattering data for atactic (80% racemic dyads) and syndiotactic forms are "virtually indistinguishable".

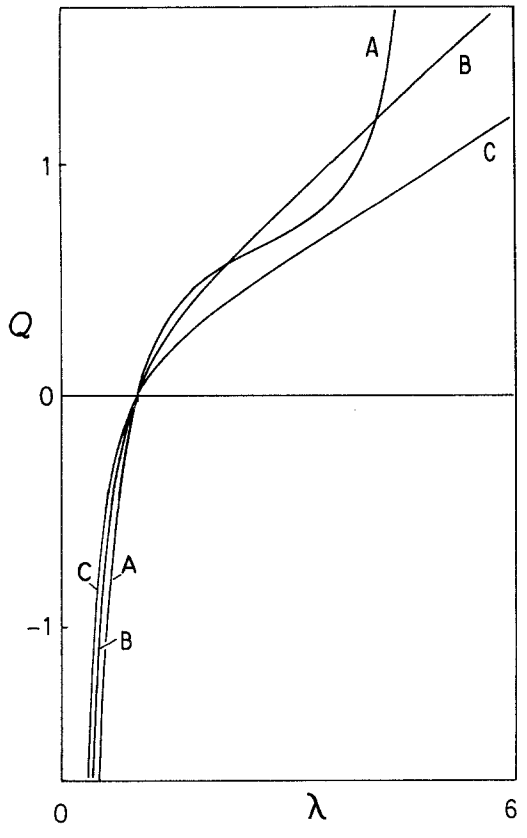

Figure 14 Comparison of model with Gaussian theory for uniaxial tension and compression. (A) two-mode model (aspect ratio 3, $K = 3$); (B) Gaussian ($NkT = 0.39$ MPa); (C) Gaussian ($NkT = 0.273$ MPa). The Gaussian plots are scaled by putting $T = 20°$ C and assuming $v = 3.0\,\text{nm}^3$. Each unit of Q would then represent 1.35 MPa.

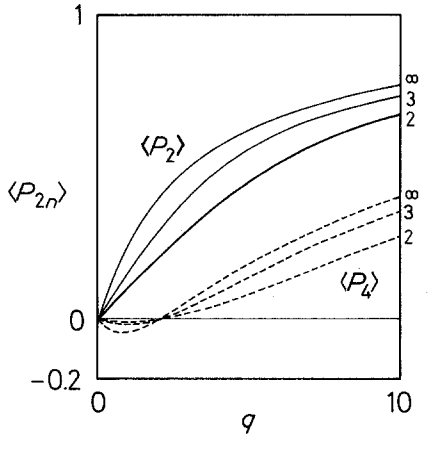

Figure 15 Variation with true stress parameter q of the first two even order spherical harmonics. Solid lines $\langle P_2(\cos\phi)\rangle$; dashed lines $\langle P_4(\cos\phi)\rangle$. Number denotes aspect ratio.

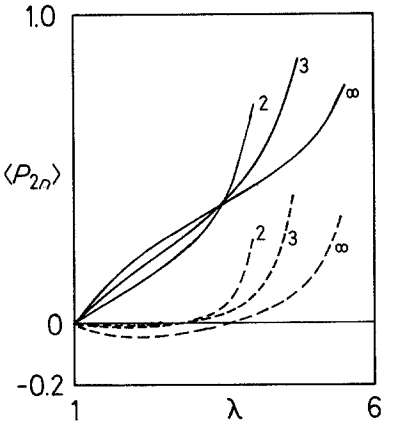

Figure 16 Effect of aspect ratio on orientation–strain plots, for the case $K = 3$. Solid lines: $\langle P_2(\cos\phi)\rangle$, dashed lines: $\langle P_4(\cos\phi)\rangle$. Number denotes aspect ratio.

by the product of initial modulus and SSOC. Fig. 16 depicts the behaviour of the first three spherical harmonics as functions of λ for the parameters chosen earlier. The most prominent difference from conventional models is that $\langle P_4\rangle$ and $\langle P_6\rangle$ become negative at low strains: the maximum negative $\langle P_4\rangle$ increases with aspect ratio, but the "cross-over" is at a fixed value of q ($q = 2$). This may help to explain negative $\langle P_4\rangle$ values reported in the literature [4–6].

2.2. Energy band representation

The "energy states" argument, used above in developing an expression for the extensional mode of deformation, can be extended to provide a means of visualizing the model in terms common to several aspects of materials science. An analogy may be drawn with a system in which a set of particles is distributed over the following energy states, as depicted in Fig. 17:

(i) a state of fixed energy (arbitrarily taken as zero energy) representing "units absent from the sampling plane";

(ii) a "band" of energy states, representing "units present in the sampling plane", with energies dependent on ϕ and on stress.

At zero stress ($q = 0$) the energy band will collapse to a delta function at the arbitrary zero of energy, and the distribution over the states will depend only on the available sites, since all states will have the same energy. At finite q, the band will begin at energy qkT (because from Equation 14, with $q' = q$, this is the energy difference between a unit absent from the plane and one

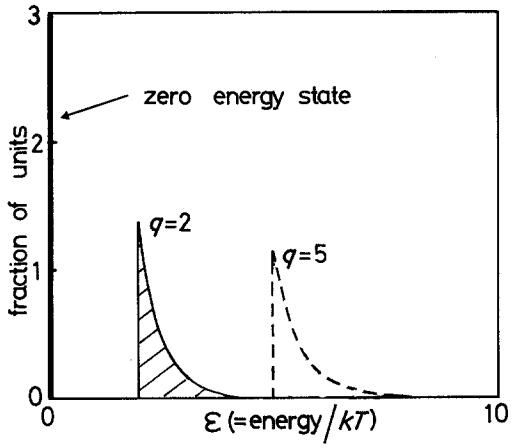

Figure 17 Energy band representation of a sampling plane in the two-mode model (aspect ratio 3, $K = 3$) for the case $q = 2$. A higher stress would shift the band to higher energies: the case $q = 5$ is shown dashed.

present but with $\phi = 0$) and will extend to an energy corresponding to a unit at $\phi = \pi/2$. For the "first approximation" model this latter energy will be infinite, because the intercept area between a unit of infinite aspect ratio and the sampling plane tends to infinity as ϕ approaches $\pi/2$. From Equation 3, the energy will vary as $(-\log\cos\phi)$. For units of finite aspect ratio, the energy will vary as $[-\log(1-e^2\sin^2\phi)]$ (cf. Appendix I), where e denotes the eccentricity of the unit. The limit as ϕ approaches $\pi/2$ is hence now finite. The effect of increasing stress is then to widen the gap between the "zero energy state" and the band, but to widen the band itself. For a given stress at a particular temperature, the cross-sectional area of the assemblage, and thus the strain, will be determined by the occupancy of the states. If there were no limit on the number of units which could be "absent" from a section at any finite stress, they would all be absent and the distribution would collapse at the zero of energy. Constraint effectively limits the occupation of the zero energy states to a finite fraction of the number of units available.

3. The model in comparison with experiment

We now re-examine some of the available experimental data in the light of the two-component model. It is beyond the scope of this series of papers to apply the nodel to all aspects of non-crystalline polymer deformation, but a more restricted examination will serve to clarify the scope and limitations of the two-mode approach.

In doing this it is appropriate to give rather more weight to orientational than to mechanical behaviour: orientation is arguably less difficult to "deconvolute" from factors of experimental geometry, technique and temperature, particularly as a variety of experimental techniques are applicable to orientation measurement and can be correlated with one another. Moreover, orientation is rather more informative about the local disposition of molecular segments*: especially so if the investigation is extended to spherical harmonics of order higher than $\langle P_2(\cos\phi)\rangle$.

Before proceeding further one should recall the formidable potency of adjustable parameters, and it is salutary to attach progressively less significance to a model as more such parameters are introduced.

For the model developed above, there are two parameters affecting the shape of the stress–strain plot: the unit aspect ratio, connected with the orientational mode, and the "constraint parameter" K, related to the extensional deformation mode, with the "average fractional constraint" on a unit equal to $1/K$. Both allow a simple first-approximation estimate to be made: molecular considerations such as chain stiffness may suggest a reasonable estimate for aspect ratio, while the maximum extension ratio – roughly estimable by extrapolation of a stress–strain curve – is controlled by both aspect ratio and K. The scaling factor v merely affects the conversion from the dimensionless units of q or Q to those of stress.

Though the characteristic shape of the stress–strain curve is probably the best known feature of rubbery behaviour, the strong sensitivity of the inflexion point to experimental conditions, e.g. via stress-softening, militates against its use as a characteristic of the deformation. The initial (static) modulus – in the uniaxial geometry, Young's modulus – is often used to characterize the mechanical behaviour of a material. In the Gaussian model it is given by $3NkT$ (in the usual notation); though the well-known "front factor" problem involves debate concerning whether the numerical factor of 3 is correct. The two-mode model predicts that the initial slope D_{q0} of the

*Or at least, the disposition of something: probably the most intractable question in orientation studies of non-crystalline systems is the nature of the "something".

Q against λ plot will be affected by both of the adjustable parameters: it will be raised by decreasing the unit aspect ratio, or by increasing the mean constraint on extensional deformation (in fact D_{q0} increases approximately linearly with $1/K$)

The parameters involved in any model designed to describe polymer behaviour should be related, if possible, to the real macromolecular chain. To this we consider several specific polymers, and start by considering the initial gradients of the stress–strain, orientation–stress and orientation–strain curves, since these afford preliminary estimates of the model parameters.

3.1. Initial behaviour: estimating the unit volume and aspect ratio

The volume v associated with a repeat unit may be calculated from density ρ and repeat unit mass M_{ru}, in atomic mass units, using the following formula, (where $N_a = 6.02 \times 10^{26}$):

$$v = \frac{M_{ru}}{\rho N_a} \tag{36}$$

In the two-mode model, given the values of the two adjustable parameters, the volume per unit may be predicted – with the reservations outlined above – from the initial slope of a plot either of Q against λ or of $\langle P_2 \rangle$ against q. The starting slope of the q–λ and Q–λ plots are of course identical. Thus for the Q against λ plot:

$$v = kT(D_{q0}/G_0) \tag{37}$$

where D_{q0} is the dimensionless slope $(dq/d\lambda)$ calculated from the model and G_0 is the modulus determined experimentally, in units of stress (in this nomenclature, G_0 is the *uniaxial* modulus, corresponding to the $3NkT$ of the elementary Gaussian theory; some authors denote the "rubber modulus" NkT by G). This provides a simple technique for estimating v on the basis of the model: we take an experimental curve, set aspect ratio and K such that the maximum strain, modulus ratio and inflexion strain approximately match those determined from experiment, and then determine v according to Equation 37.

Alternatively, the initial slope of the $\langle P_2 \rangle$–stress plot (denoted SQOC) is related to the conventional stress–optical coefficient (SSOC) via v:

$$v = \frac{kT}{\Delta\mu_0} \frac{\text{SSOC}}{\text{SQOC}} \tag{38}$$

where $\Delta\mu_0$ is the intrinsic (maximum orientational) birefringence.

The second method differs from the first in that the SQOC should be independent of the extensional mode and hence of K. Data for SSOC are rarely directly available: they are generally obtained under load, so that birefringence will be composed of both stress-related and orientation-related contributions. Ideally, one would work with data obtained by a quench–unload procedure: even then, however, there is a risk of quenching in some stress birefrigence, particularly in view of the sharp rise in stress on quenching through the glass transition in anything but a perfectly "soft" testing apparatus. Stress-optical data can frequently be obtained only by combining strain-optical coefficient (SNOC) and initial modulus measurements from different samples or even different investigations, thus introducing a possible source of error.

Combination of Equations 37 and 38 leads to an expression for the strain-optical coefficient (SNOC), which is independent of v:

$$\frac{d\langle P_2 \rangle}{d\lambda} = \frac{\text{SNOC}}{\Delta\mu_0} = \frac{G_0 \text{SSOC}}{\Delta\mu_0} = D_{q0}\text{SQOC} \tag{39}$$

We will abbreviate $d\langle P_2 \rangle/d\lambda$ to SNOCP. It is convenient to plot the reciprocal initial slope of the stress–strain curve, $1/D_{q0}$, against SQOC, since a fixed value of strain-optical coefficient will correspond to a straight line through the origin on such a plot.

This gives us a procedure (Fig. 18) for fitting values of the model parameters to the initial strain-optical behaviour of a real material. We first draw the staight line referred to above, of gradient equal to SNOCP. This cuts through the set of curves corresponding to particular values of K and if we have estimated "plausible limits" on K, we may determine the corresponding limiting pairs of values of (D_{q0}, SQOC). The SQOC is dependent only on the unit aspect ratio, so that the corresponding range of possible aspect ratios may also be determined. The aspect ratio tells us the maximum orientational strain λ_0^{max} and hence, multiplying λ_0^{max} by K, the maximum overall extension ration λ_{max}. Reference to a stress–strain curve will indicate what λ_{max} is reasonable, and we can then select a reasonable pair of values of aspect ratio and constraint parameter within our possible range (we could alternatively use some

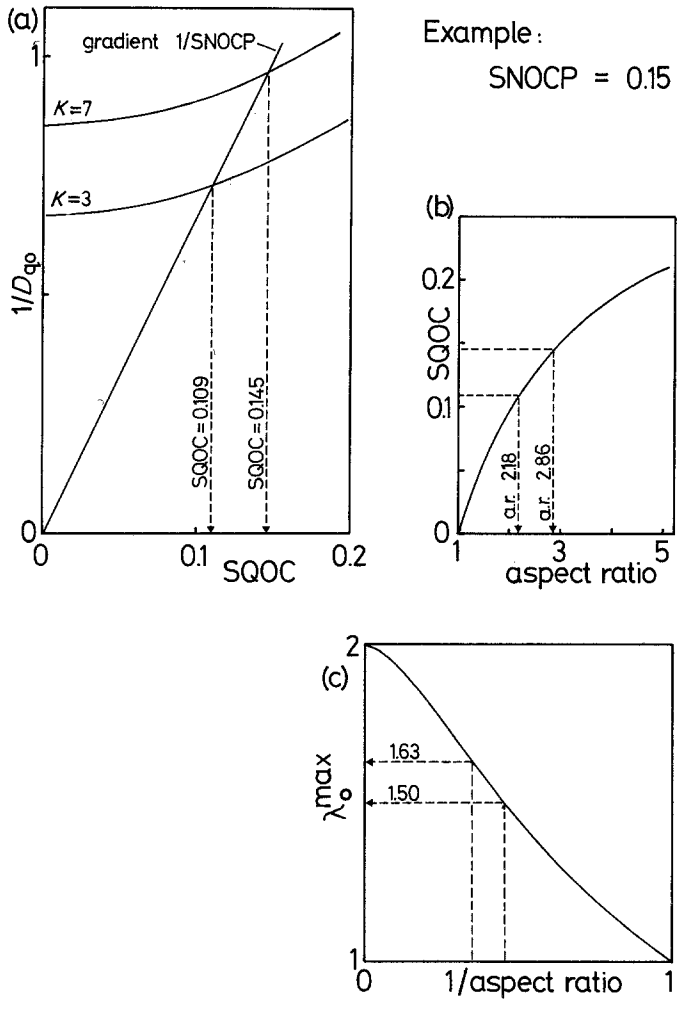

Figure 18 Interpretation of strain-optical coefficient SNOCP = $d\langle P_2\rangle/d\lambda$. Assume plausible values of K to lie in the range 3 to 7. (a) Determine SQOC for limiting values of K; (b) determine aspect ratio from SQOC; (c) determine λ_0^{max} from aspect ratio (use of reciprocal aspect ratio reduces plot curvature). Maximum strains ($\lambda_0^{max}K$): $1.50 \times 3 = 4.50$, $1.63 \times 7 = 11.41$.

other characteristic property instaed of λ_{max} to see which values within the range appear most appropriate).

The procedure is illustrated by Fig. 18 for a hypothetical example where SNOCP = 0.15, with K required to be in the range 3 to 7. From Fig. 18a the line cuts the $K = 3$, $K = 7$ curves at SQOC = 0.109, 0.145, resepctively. These values correspond (Fig. 18b) to aspect ratios 2.18, 2.86; to λ_0^{max} of 1.50, 1.63; and to overall maximum extension ratios of 4.49 and 11.44 respectively. The use of the λ_0^{max} against reciprocal aspect ratio diagram (Fig. 18c) provides a nearly linear plot which is convenient to use. SNOCP values will typically be taken from tangents on published diagrams, so that deductions from them should be regarded as approximate.

With this type of analysis of initial orientation–strain behaviour as a starting point, we can go on to consider some individual polymers which, given suitable regimes of temperature and experimental time-scale, exhibit rubber-like behaviour. It is appropriate to concentrate on materials in which orientation has been studied using a variety of techniques, allowing $\langle P_2(\cos\phi)\rangle$ to be monitored without relying entirely on rather uncertain estimates of such quantities as intrinsic birefringence.

3.2. Poly(ethylene terephthalate)

The commercial use of poly(ethylene terephthalate) (PET) as oriented film and fibre provides a stimulus for the study of its mechanical and orientational changes during deformation. Several techniques have been applied to the investigation of orientation–strain relationships, including a useful body of data obtained at Leeds University, UK, on material of near-zero crystallinity drawn at 80° C [7–11]. Quoted values for SNOCP from

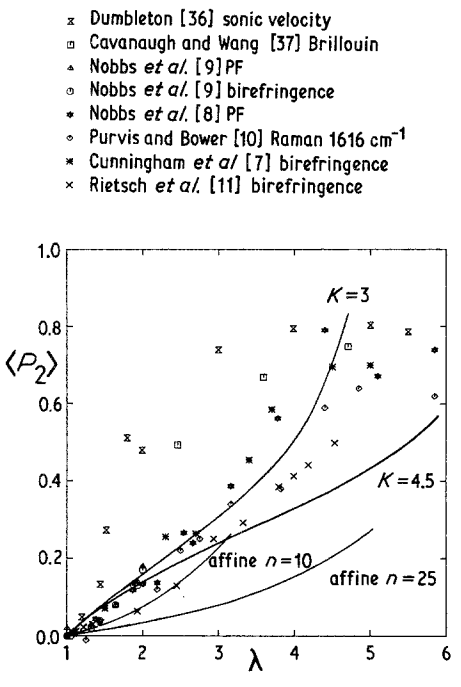

Figure 19 PET orientation data compared to affine and two-mode (aspect ratio 3) predictions. All data refer to a draw temperature of 80° C.

these data include:

Cunningham *et al.* [7] (i.r. spectroscopy birefringence)	0.107
Nobbs *et al.* [8] (polarized fluorescence)	0.072
Purvis and Bower [10] (laser-Raman spectroscopy)	0.17
Rietsch *et al.* [11] (birefringence)	0.072

The result of Rietsch *et al.* assumes an intrinsic birefringence of 0.235 [12]. While their result agrees with that of Nobbs *et al.*, Rietsch *et al.* plot birefringence data obtained by other workers and show that most strain-optical coefficients would be somewhat higher – giving SNOCPs up to perhaps 0.35.

A plot of the available data (Fig. 19) indicates that a representative figure for SNOCP would be nearer to the 0.17 of Purvis and Bower [10], judging from the "steady" slope of the plot over the first 200% or so of strain. In making this assessment we leave aside data which, though from supposedly non-crystalline material, displays even above T_g the pseudo-affine orientation behaviour typical of crystallites: such data is examined elsewhere [13]. The value 0.17 lead to:

at $K = 3$: SQOC = 0.128, aspect ratio 2.51
$\lambda_0^{max} = 1.572$, $\lambda_{max} = 4.72$

at $K = 7$: SQOC = 0.172, aspect ratio 3.56,
$\lambda_0^{max} = 1.725$, $\lambda_{max} = 12.07$

An intermediate case of aspect ratio 3 requires $K \simeq 4.25$ for this SNOCP and leads to $\lambda_{max} \simeq 7.0$.

In view of the uncertainty over the initial slope, it is worth trying to improve the fit by looking at the full $\langle P_2 \rangle$–strain curve, and reducing K to 3 gives the fit shown by the solid line in Fig. 19. It is fortuitous that this approximate fit (aspect ratio 3, $K = 3$) coincides with the parameter values suggested above: obviously there is room for refinement, but the scatter in the orientation–strain data and the absence of corresponding stress–strain curves means that attempts at greater precision is not really justified.

At high strains, data points tend to lie on the high-strain side of the model prediction, and this may indicate that the best choice of parameters will change with increasing strain; which is what we might have expected, bearing in mind the conformational changes which come into play [13]. Fig. 19 also shows, for comparison, the affine predictions for $n = 10$ and $n = 25$. Even with a value as low as $n = 10$, the curve still falls below most of the data; and $n = 10$ implies a limiting sttrain of only $\lambda_{max} = 10^{1/2} \simeq 3.16$ under affine deformation. Furthermore, Cunningham *et al.* [7] find evidence for the existence of a unique relationship between $\langle P_2 \rangle$ and the proportion of *trans* conformers: this correlation continues to hold beyond $\lambda = 10^{1/2}$, which seems to indicate that there is no change in mechanism associated with the "affine limit".

The nearest we can get to a stress–strain curve for the material considered above is the peak shrinkage stress again strain plot recorded by Rietsch *et al.* [11], reproduced in Fig. 20 (note that the abscissa is $\lambda^2 - 1/\lambda$). The apparent maximum strain agrees well with the model prediction of $\lambda_{max} \simeq 5$, and the initial slope of the stress–strain curve can be matched to that of Rietsch *et al.*'s plot by taking the volume per unit to be approximately 0.929 nm^3, equivalent to some 3.8 repeat units. This is only slightly greater than the 2.9 repeat units per equivalent random link which Cunningham *et al.* [7] require in order to fit low-strain $\langle P_2 \rangle$ data by an affine model.

The parameters above, and this estimate of v, allow one to draw an ellipsoid to represent to a

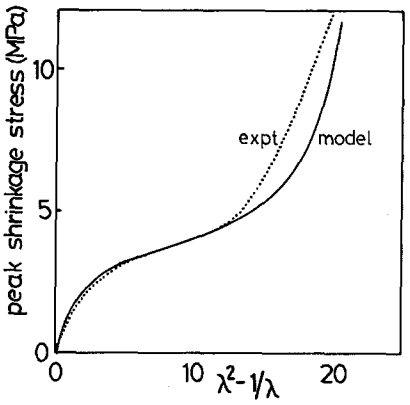

Figure 20 Nominal stress–strain curve from two-mode model (aspect ratio 3, $K = 3$) compared to shrinkage stress against strain plot for PET from Rietsch *et al.* [11]. The vertical scaling assumes $v = 0.929\,nm^3$.

first approximation the orienting unit for PET. Fig. 21 shows such an ellipsoid in comparison to the PET chain, assuming a packing density of 0.6 (i.e. volume of the ellipsoid alone = $0.550\,nm^3$). It should be emphasized that the ellipsoid will be an idealized representation of the "typical" orienting unit, and clearly, because of the nature of the chain packing, it would be misleading to try and draw discrete units with clearly defined boundaries. Nevertheless, the case of PET gives grounds for believing that the two-mode model offers a worthwhile approach to orientational deformation, at least in the regime where rate effects may be neglected.

3.3. Poly(methyl methacrylate)

Poly(methyl methacrylate) (PMMA) is perhaps the best non-crystalline polymer for mechanical and

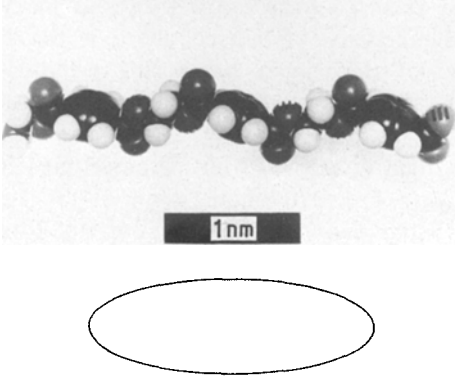

Figure 21 Suggested idealised orienting unit for PET compared to a space-filling model of the molecular chain. Aspect ratio 3; volume of ellipsoid $0.550\,nm^3$; packing density 0.6.

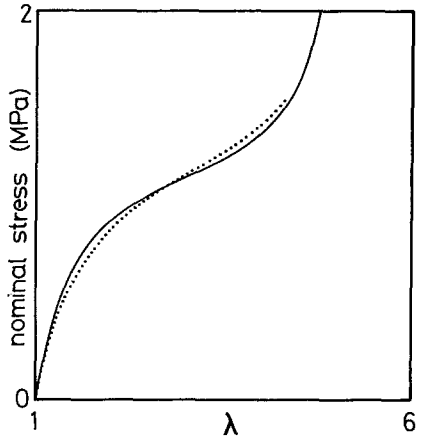

Figure 22 Fitting the experimental stress strain curve for PMMA in uniaxial tension at 150° C. Aspect ratio 1.46, $K = 4.5$. Scaling: $v = 3.150\,nm^3$. Experimental curve is dotted.

orientation studies. It is well-characterized, free from strain-induced crystallization, optically transparent, and fairly well-understood from a structural viewpoint [3].

At 150° C, well above the glass transition of around 105° C, it has an initial Young's modulus of approximately 1.6 MPa and an SNOCP of about 0.067, without correction for irrecoverable flow (of order 10% of the measured true strain at $\lambda \simeq 4$) The latter leads to:

at $K = 3$: SQOC = 0.046, aspect ratio 1.39,
$\lambda_0^{max} = 1.22$, $\lambda_{max} = 3.66$

at $K = 7$: SQOC = 0.059, aspect ratio 1.53,
$\lambda_0^{max} = 1.28$, $\lambda_{max} = 8.98$

To obtain a maximum strain comparable to that indicated by experiment we take an intermediate case: aspect ratio 1.46, $K = 4.5$ gives $\lambda_{max} \simeq 5.6$, which is in agreement with the stress–strain curve in Fig. 22.

The same choice of parameters gives a satisfactory fit to the 150° C orientation–strain data up to strains of 250% to 300% ($\lambda = 3.5$ to 4), as shown in Fig. 23.

These data do not in themselves provide evidence for the predicted upturn in the $\langle P_2 \rangle$–strain plot at still higher strains. The highest-strain point may in fact be an indication of a departure from the predicted curve: a reason for this is suggested by recalling (cf. Part 1) that orientation is more susceptible to recovery than is overall strain. The 150° C deformation was performed rapidly (some tens of seconds); but a further few

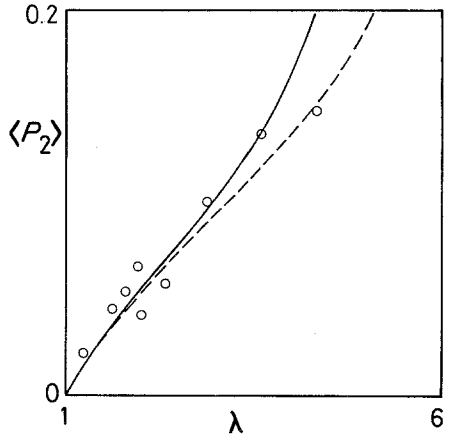

Figure 23 Predicted orientation–strain relationship compared to WAXS data (circles) for PMMA in uniaxial tension at 150° C. Solid line: aspect ratio 1.46, $K = 4.5$. Dashed line: aspect ratio 1.5, $K = 5.6$.

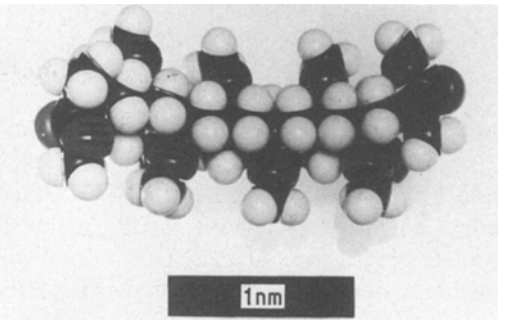

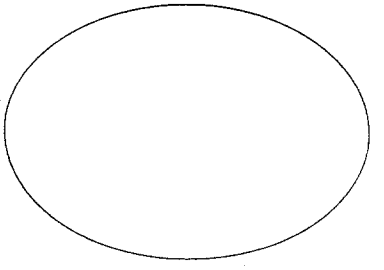

Figure 24 Suggested idealized orienting unit for PMMA compared to a space-filling model of the molecular chain. Aspect ratio 1.46; volume of ellipsoid 1.890 nm^3; packing density 0.6. The photograph was taken normal to the ester sidegroups.

seconds elapsed while the specimen, under load, was cooled to below T_g (as judged by the sudden rise in load). It may well be during this initial cooling that any recovery of orientation takes place, with the less easily recovered extensional mode making up for the loss of orientational deformation. This too would be particularly significant at high stresses (and hence high strains), and might therefore explain the absence of the expected upturn in the $\langle P_2 \rangle$–strain plot above $\lambda \simeq 4$.

A similar observation applies to the plane strain results of Pick and co-workers [6, 14, 15] where higher strains were achieved than in the uniaxial work. There is little evidence of an upturn (the slight upturn in Pick's 150° C curve is due to an isolated point at $\lambda \simeq 7.5$). One might expect the cooling problem to be more significant here: the nature of the plane strain geometry, with metal dies in contact with the specimen, means that cooling will be slower owing to the heat capacity of the apparatus. The stress–strain curve in Fig. 22, obtained during loading, does of course display the predicted upturn.

The selection of aspect ratio 1.46 from the range allowed by the experimental SNOCP, though rather arbitrary, appears to fit the $\langle P_2 \rangle$–strain behaviour reasonably successfully up to moderate strains. It is worth noting that a slightly different choice can be made to fit $\langle P_2 \rangle$ up to higher strains: Fig. 23 also gives the case of aspect ratio 1.5, which for the same SNOCP requires $K = 5.6$. The corresponding stress–strain curve, however, exhibits too pronounced an inflexion to allow as close a fit to its experimental counterpart as the earlier pair of parameters: which further underlines the importance of giving attention to both orientational and stress–strain behaviour in assessing a model.

As in the case of PET we can now arrive at some specific information on the dimensions of the effective (idealized) orienting unit. The fit to the stress–strain curve (Fig. 22) assumes a volume per unit v of 3.150 nm^3, corresponding to some 22 repeat units or 2 to 3 times the length of Lovell and Windle's runs of uniform conformation.

This volume, with the aspect ratio of 1.46, gives the ellipsoid shown in comparison to the PMMA chain in Fig. 24 (again for a packing density of 0.6). The aspect ratio is much smaller than for PET, which is perhaps to be expected since the cross-section of the PMMA chain is considerably greater than that of PET, especially when taken in comparison to the monomer repeat distance. The size, in comparison to the typical run of uniform conformation, is plausible too: it points to such segments not quite moving independently, but interacting with their neighbours such that motion is "correlated" over a region encompassing the equivalent of two to three segments. We conclude

that the idealized orienting unit for PMMA appears to be plausible in molecular terms.

3.4. Poly(vinyl chloride)

The development of orientation as measured by $\langle P_2 \rangle$ with strain in poly(vinyl chloride) (PVC) is rapid even above T_g. Taking the 110° C data of Hibi *et al.* [16] for unplasticized PVC, with their estimate of $\Delta\mu_0$, we obtain SNOCP $\simeq 0.61$, which matches almost exactly the pseudo-affine SNOCP of 0.6. It would be impossible to fit the two-mode model to such a high SNOCP for any reasonable value of K (in fact, for any K above 1.06), and the close fit to the pseudo-affine scheme points strongly to crystallites as the chief source of the measured orientation. Although Hibi *et al.* regard their material as "non-crystalline", their results agree with those of Robinson *et al.* [17], which the latter authors interpret in terms of crystallite orientation.

Studies on commercial PVC [18, 19] indicate a lower SNOCP, but this may well be associated with the presence of plasticizers.

3.5. Natural rubber

The properties of natural rubber vary greatly depending on the method of preparation and the (often complex) composition of the material. The initial modulus varies according to cross-link density, but typical values would lie in the range 1 to 2 MPa [20–27], and such values would point on the basis of Equation 37 to a unit volume of some few cubic nanometres, i.e., some tens of repeat units.

Optical orientation data are more difficult to interpret. Values for the stress-optical coefficient will include both stress-related and orientation-related contributions, while considerable uncertainty remains over the magnitude of the intrinsic birefringence, so that it is not possible to test the model in detail for natural rubber at this stage. Treloar [28] reports a value of 0.0945 for the highest birefringence observed experimentally (under load) but calculates an intrinsic birefringence of 0.28 on the basis of a theoretical treatment of the isoprene structure. However, Treloar's assumptions are such that the calculation can only be a first approximation. Nevertheless, we may with reasonable confidence say that the SNOCP of natural rubber will be small in comparison to those of other polymers, indicating a unit aspect ratio not far above 1 and hence a relatively small orientational contribution to deformation when viewed in the context of a broad range of polymers. Indeed, natural rubber can be misleading unless it is so viewed.

The strain-induced crystallization of natural rubber will become particularly significant at high strains, but it is difficult to determine a level of strain below which it can be neglected (if indeed there is one); although initial slopes should be unaffected unless the starting material is partially crystalline in the as-received condition. The stress-softening or Mullins effect presents a further problem. Several workers take care to subject their samples to prior deformation so that the main experiment will be performed on "stress-softened" material: however, since stress-softening is both incompletely understood and (more importantly) subject to partial relaxation with time, it may still affect the results to an indeterminate degree. For reasons such as these, the behaviour of natural rubber should probably be given rather less weight than that of better-characterized polymers.

3.6. Styrene–butadiene rubbers

Styrene–butadiene rubbers (SBRs) are a commercially important group of copolymers. Some difficulty might be anticipated in the modelling of copolymer behaviour, since the two monomer units do not occur in any fixed sequence, and parameters such as effective unit size and aspect ratio might be expected to vary more than in a homopolymer. The modulus will depend on the ratio of the constituents as well as on cross-linking: Morgan and Treloar [27] record data which indicate moduli ranging from 0.8 to 5.1 MPa.

The Kuhn–Grün theory for the optical behaviour of rubbers has been generalized by Shindo and Stein [29] to systems with more than one type of statistical segment, though even when their modified theory is applied to polybutadiene (where the two types of segment are effectively the *cis* and *trans* conformers, and are thus not very dissimilar) there is some discrepancy between results from unswollen and solvent-swollen material. The stress-optical coefficient falls as the proportion of styrene is increased [27], but to follow the corresponding trend in v would require a knowledge of the variation of intrinsic birefringence as well.

Doherty *et al.* [30] make concurrent measurements of stress, strain and birefringence: their birefringence–stress graph (their "Fig. 3") suggests

a maximum birefringence near 2.5×10^{-2} – though this will include both stress and orientation components. If we neglect the stress birefringence, we obtain (for the 0° C data):

$$G_0 \simeq 0.45\,\text{MPa}$$

$$\text{SSOC} \simeq 3.2 \times 10^{-9}\,\text{Pa}^{-1}$$

$$\text{SNOCP} \simeq 5.7 \times 10^{-2}$$

Using the procedure given above, we obtain an aspect ratio ranging from 1.27 at $K = 3$ ($\lambda_0^{\max} = 1.16$, $\lambda_{\max} = 3.48$) to 1.36 at $K = 7$ ($\lambda_0^{\max} = 1.21$, $\lambda_{\max} = 8.44$). A choice of K near to the latter would give a maximum strain similar to that found experimentally (Doherty *et al.*'s "Fig. 1"), i.e. about $L = 8$. The $K = 7$ parameters would also indicate $D_{qo} \simeq 1.15$, and hence $v \simeq 9.650\,\text{nm}^3$; for comparison, the monomer repeat unit volumes are $0.094\,\text{nm}^3$ for butadiene and $0.165\,\text{nm}^3$ for styrene.

The Shindo–Stein copolymer analysis is not applied by Doherty *et al.* to their results. They do apply a "conventional" non-Gaussian analysis (following Treloar and Riding [31, 32]), but obtain what would appear to be rather poor agreement with stress–strain (their 'Fig. 1") and birefringence-strain ("Fig. 2") data. The SBR is a worthwhile system to study, in comparison to natural rubber, since crystallization is absent; it is nonetheless noteworthy that the upturn in the stress–strain curve at high strains remains clearly visible.

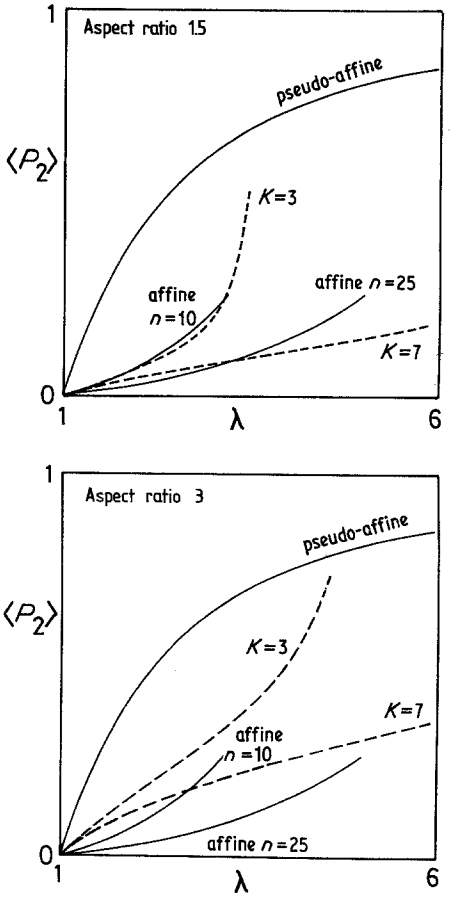

Figure 25 Orientation–strain relationship predicted by the two-mode model (dashed curves) in comparison to other deformation schemes.

3.7. Comparison with conventional models

The expressions for $\langle P_2(\cos\phi)\rangle$ given by, for example, Nobbs and Bower [33], allow the affine SNOCP to be calculated easily for a chain of n equivalent random links. To match such a calculation to experiment will, as anticipated in Part 1, often require a value for n which is both variable and, at low strains, very small. The estimate of SNOCP for a styrene–butadiene rubber given above would suggest $n \simeq 11$ (neglecting any stress birefringence), while the data for PMMA and PET discussed above point to $n < 10$, which calls into question the applicability of an affine statistical approach. Natural rubber can now be seen as something of an exception to the general picture, requiring a reasonably large n (some tens of links, depending on the intrinsic birefringence assumed).

The pseudo-affine deformation scheme predicts a fixed SNOCP of 0.6, well above anything which the two-mode model as so far developed could predict with plausible values for aspect ratio and constraint. However, it is below the glass transition, where time and strain rate become important, that the pseudo-affine scheme is of most use with non-crystalline polymers. The introduction of rate effects into the two-mode model would lead to greatly increased SNOCPs; but that is the subject of Part 3 [34].

Going to moderate strains, we first underline that the upturn in the stress–strain curve, and the finite limiting extension ratio, are inherent and indeed fundamental features of the two-model model, even at its simplest stage of development – an important contrast to the Gaussian model which represents the affine approach in its simplest form. The $\langle P_2\rangle$–strain plot is, as illustrated by Fig. 25, intermediate between the pseudo-affine and typical affine predictions. The slope at low strain increases markedly with increasing con-

straint (decreasing K) and – less markedly – with increasing aspect ratio. $\langle P_4 \rangle$ and higher order Legendre polynomials are discussed below: they remain near zero until the limiting strain is approached, and a tendency to small negative values of $\langle P_4 \rangle$ is most apparent at larger aspect ratios (cf. Fig. 27).

All the $\langle P_{2n} \rangle$–strain plots have the advantage of being independent of the volume v per orienting unit: they are thus a particularly useful measure of the behaviour of the two-mode model.

3.8. Cross-link density

The orientational component of deformation, and hence the orientation–true stress relationships, are independent of the constraint parameter K (except in a secondary way via any "coupling" between the two deformation modes). This fact corresponds to the experimental observation that the stress-optical coefficient is, to a first approximation, independent of cross-link density. The relationship of K to the effective density of cross-links ("mechanical" as well as "chemical") is discussed in Appendix II, where it is suggested that an analogue of cross-link density is the quantity $K^{-3/2}$.

With this suggestion, we make the observation that plausible values of the model parameters lie in a range where an approximately linear relationship between $K^{-3/2}$ and the initial modulus holds (Fig. 26) – in agreement with the experimentally observed relationship between modulus and cross-link density.

3.9. Higher order spherical harmonics

Conventional models for rubber-like deformation, based on the affine assumption, predict low positive values of $\langle P_4(\cos\phi) \rangle$ in uniaxial tension at all strain up to the $n^{1/2}$ limit. The relatively few experimental data available (e.g. [5, 6] for PMMA) indicate that $\langle P_4 \rangle$ does indeed remain low even at high strains. However, the negative sign of some of the experimentally-determined values of $\langle P_4 \rangle$, particularly at low strains, does not accord with the affine scheme.

The relationship between $\langle P_4 \rangle$ and $\langle P_2 \rangle$ is a useful characteristic of a deformation scheme, showing – at least in the uniaxial geometry – little dependence on the affine n and no dependence on the parameter K in the two-mode model. The relationship is shown, for low degrees of orientation, in Fig. 27. In general the two-mode model

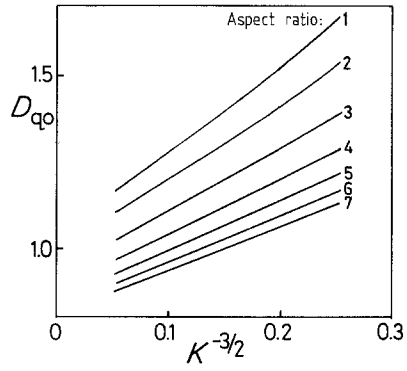

Figure 26 Initial modulus (in units of q) D_{q0} against $K^{-3/2}$. The abscissa is analogous to a measure of cross-link density.

predicts lower $\langle P_4 \rangle$ for given $\langle P_2 \rangle$ than the affine and pseudo-affine schemes; though this effect, together with the tendency for early $\langle P_4 \rangle$ values to be negative, becomes less marked as the unit aspect ratio approaches 1. Only limited data for $\langle P_4 \rangle$ against $\langle P_2 \rangle$ are available, and unfortunately some of the samples were of unknown strain. The alternative practice of plotting $\langle \cos^4\phi \rangle$ against $\langle \cos^2\phi \rangle$ is less useful, since the plots discriminate less well between alternative deformation schemes.

Data for PVC are shown in Fig. 28. There are few points present, but they fall close to the affine and pseudo-affine predictions rather than to that of the two-mode model. However, "pseudo-affine" behaviour may be connected with the possible presence of crystallites in the PVC [17].

The behaviour of $\langle P_4 \rangle$ for PET has been studied by polarized fluorescence [8, 9] and laser-Raman techniques [10]. The latter method is subject to the usual uncertainties concerning line assignment

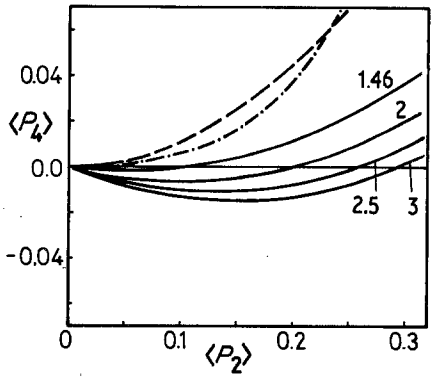

Figure 27 $\langle P_4(\cos\phi) \rangle$ against $\langle P_2(\cos\phi) \rangle$ for the two-mode model and other deformation schemes. – – – pseudo-affine, –·–·– affine ($n = 25$), —— two-mode (number denotes aspect ratio).

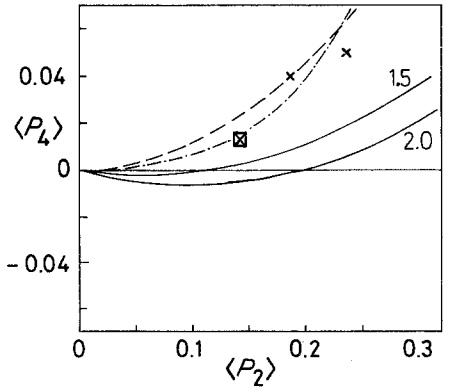

Figure 28 $\langle P_4(\cos\phi)\rangle$ against $\langle P_2(\cos\phi)\rangle$ for PVC (Kashiwagi and Ward [35]; NMR). Temperatures: ⊠ 90° C; × 80° C. Curves as in Fig. 27.

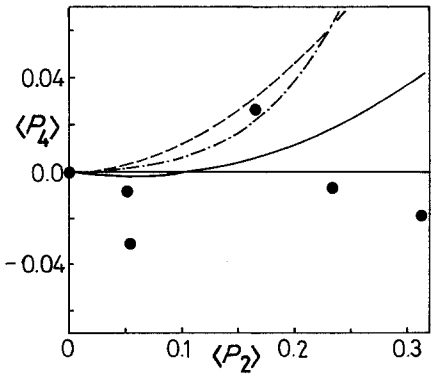

Figure 30 $\langle P_4(\cos\phi)\rangle$ against $\langle P_2(\cos\phi)\rangle$ for PMMA drawn at temperatures in the range 115 to 160° C (Kashiwagi *et al.* [4]; NMR). -·-· affine ($n = 25$); – – – pseudo-affine; —— two-mode (aspect ratio 1.46).

and the Raman tensor: for some lines impossible values of $\langle P_4\rangle$ were obtained. Fig. 29 shows results based on the 1616 cm^{-1} line, regarded by the authors as the most useful. Most of the $\langle P_4\rangle$ values so obtained exceed even the pseudo-affine prediction, with the exception of those at high strain, which lie between the pseudo-affine and two-mode predictions. However, it will be noted below that laser-Raman values of $\langle P_4\rangle$ for PMMA fail to agree with those from NMR and WAXS: the technique should therefore be treated with reserve so far as $\langle P_4\rangle$ is concerned.

The PF data for PET (Fig. 29) lie close to the pseudo-affine curve, but Nobbs *et al.* [8] suggest

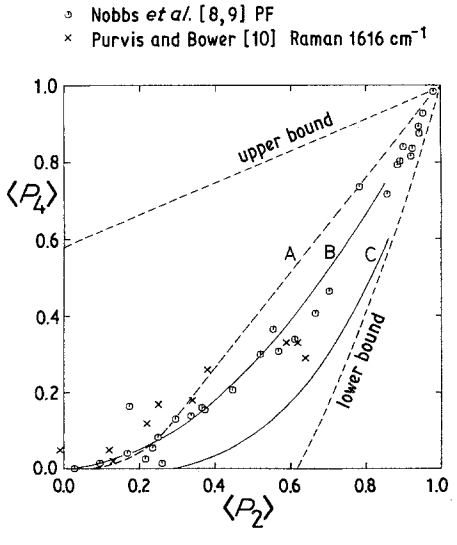

Figure 29 $\langle P_4(\cos\phi)\rangle$ against $\langle P_2(\cos\phi)\rangle$ for PET drawn at 80° C. (A) Affine ($n = 25$, but all $n > 5$ are indistinguishable on this scale); (B) pseudo-affine; (C) two-mode (aspect ratio 3).

that this may be fortuitous, since no allowance was made for the fact that the fluorescent molecules do not necessarily lie parallel to the polymer backbone chains. They deduce that that fluorescent molecules tend to be more highly oriented than the chains. If this is so, the $\langle P_4\rangle$–$\langle P_2\rangle$ relationship need not be the same as for the chains: indeed, the fluorescent additive molecules can be visualised as akin to the "floating rods" to which the pseudo-affine model strictly applies. While these experimental data for $\langle P_4\rangle$ in relation to $\langle P_2\rangle$ do not provide support for the two-mode model, the uncertainties in both techniques preclude firm conclusions.

Data for PMMA have been obtained by WAXS, NMR and laser-Raman spectroscopy. Fig. 30 shows NMR data: scatter is considerable, but there is evidently a tendency towards negative $\langle P_4\rangle$, a possibility predicted by the two-mode model, but by neither the affine nor the pseudo-affine scheme. WAXS data (Fig. 31) again exhibit considerable

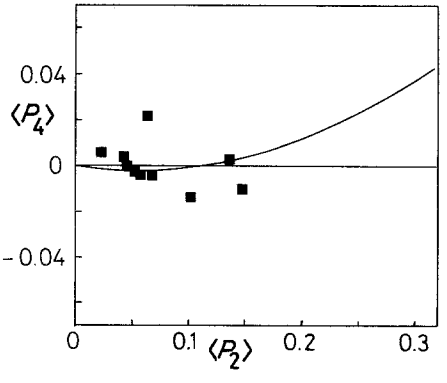

Figure 31 $\langle P_4(\cos\phi)\rangle$ against $\langle P_2(\cos\phi)\rangle$ for PMMA deformed at 150° C ([5]; WAXS).

scatter, but most points lie closer to the two-mode line than to other predictions (the solid curve corresponds to the aspect ratio of 1.46 suggested above for the orienting unit in PMMA). By contrast, the laser-Raman data of Purvis and Bower [38] would predict very much higher $\langle P_4 \rangle$, at given $\langle P_2 \rangle$, than any of the deformation schemes would predict.

In regard to $\langle P_6(\cos\phi) \rangle$, we note only that predicted values remain low at all accessible strains, in line with such experimental indications as are available.

3.10. Possible variation of average constraint with strain

It is clearly possible that the most appropriate values of the model parameters may change with stress, strain, or temperature. Indeed, it would perhaps be surprising if the "average constraint" on a mobile unit did not change with increasing deformation. Changes in aspect ratio and v are less easily visualized (except possibly for large step changes connected with a transition from "bundle" motion to independent chain motion). Small changes in v may be due to the fact that deformation is not perfectly isovolumetric. The required trend in K may be followed by considering an experimental orientation–strain plot, selecting an appropriate aspect ratio, and using an iterative method to determine, where possible, the K required to match the model to the data at each point – a procedure analogous to that employed in Part 1 to fit the affine deformation scheme to experiment by allowing a changing n, the number of equivalent random links per chain.

Taking the case of PET drawn at 80° C and again setting the unit aspect ratio to 3, we obtain the trend shown in Fig. 32. At low strains, where the values of $\langle P_2 \rangle$ are low and the predicted $\langle P_2 \rangle$–strain curves for different parameter values are close, we inevitably find considerable scatter. At moderate strains, a clear trend is visible, with the "average constraint" falling off only very slowly with increasing strain. This may be interpreted, as indicated above, in terms of the "pulling-out" of some of the intertwined chains*. One may expect this behaviour to be non-recoverable, perhaps helping to account for the irrecoverable component of strain in PMMA at 150° C. Alternatively,

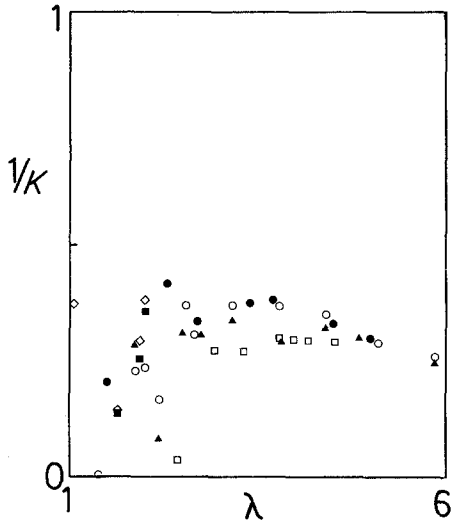

Figure 32 "Average constraint" for PET drawn at 80° C as a function of extension ratio: derived from $\langle P_2 \rangle$–strain data, assuming ratio 3. • Cunningham *et al.* [7], birefringence; ▲ Purvis and Bower [10], Raman, 1616 cm^{-1} line, "model B"; ○ Nobbs *et al.* [8], analysed as in [9], polarized fluorescence; ■ Nobbs *et al.* [9], birefringence; ◇ Nobbs *et al.* [9], PF; □ Rietsch *et al.* [11], birefringence.

as indicated above, the decline in "constraint" may be associated with an increasing ratio of *trans* to *gauche* conformers. In this case, the mean aspect ratio may also change.

Similar behaviour is shown in Fig. 33 for PMMA, taking the aspect ratio of 1.46 derived above and this time analysing data relating to various temperatures. No intrinsic birefringence figure is quoted by Shishkin and Milagin [39], but for the purposes of Fig. 33 an approximate conversion to $\langle P_2 \rangle$ has been made using a value $\Delta\mu_0 = 4.7 \times 10^{-3}$, based on NMR and WAXS studies of the UMIST series of uniaxially drawn "Perspex" specimens [4, 15].

3.11. Orientation–stress behaviour

Though the experimental $\langle P_2 \rangle$ against stress plot for typical rubbers is approximately linear at low stresses, it levels off very clearly if the range of strain is sufficient (see for example [30] on natural rubber and SBR). The two-mode model, unlike the simpler forms of the affine theory, predicts such a decrease in gradient – though a full comparison with experimental stress-optical data would be possible only if one were able to separate stress

*This cannot apply to topological entanglements rigorously defined, unless some bond scission takes place so as to allow it. Such scission is by no means impossible, though one would perhaps expect it to be significant only at high stresses.

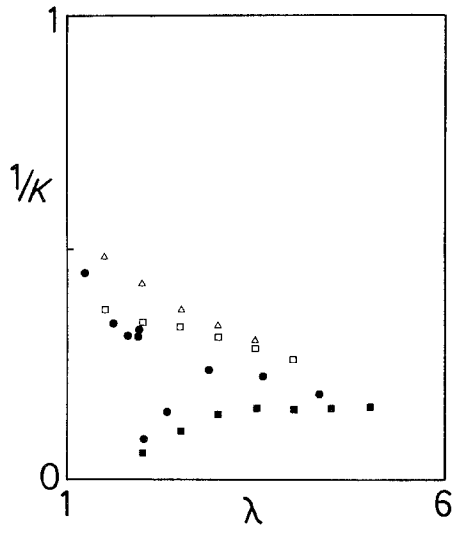

Figure 33 "Average constraint" for PMMA as a function of extension ratio: derived from $\langle P_2 \rangle$–strain data, assuming aspect ratio 1.46. • Brown and Mitchell [5], 150° C; △ Shishkin and Milagin [39] (approximate), 125° C; □ *ibid.*, 140° C; ■ *ibid.*, 190° C.

birefringence and orientation birefringence contributions.

4. Summary

The *raison d'être* for the two-component model is its potential to describe the differences between glassy and rubbery orientation–strain data. For it to be of value, it must be able to predict the deformation behaviour typical of the rubbery state at least as successfully as the existing theories. The most complete sets of stress–orientation–strain (SOS) data for rubber-like deformation refer to non-crystalline PET and PMMA above the glass transition: in each case, data obtained by a variety of techniques are available. There is some question as to whether PET at 80° C can be considered completely non-crystalline, but this problem does not arise with atactic PMMA, for which a detailed conformational model also exists. The SOS data for natural rubber are all based on birefringence measurements, which means that absolute plots of $\langle P_2 \rangle$ against strain are not available. Furthermore substantial strain-induced crystallization sets in for natural rubber extended beyond about $0.7\,\lambda_{max}$.

Figs. 19, 20, 22 and 23 show that the two-component model is able to predict the observed stress–strain and orientation–strain curves for rubbery PET and PMMA. For each polymer, the same pair of structural constants, aspect ratio and constraint parameter K, enables both types of experimental data to be fitted. This is in contrast to the affine model, where the $\langle P_2 \rangle$ against strain data can only be fitted if n, the number of equivalent random links per chain, is allowed to change drastically with strain (cf. Figs. 2 and 3 of Part 1). The values of aspect ratio of the orienting unit (approximately 3 for PET and 1.5 for PMMA) are not unreasonable in view of the likely molecular run lengths of the underlying conformations, and the characteristic volumes necessary to scale the stress–strain predictions (0.550 nm^3 for PET and 3.150 nm^3 for PMMA) are also molecularly reasonable. It thus appears that the two-component approach is able to predict the rubber behaviour of PET and PMMA rather better than the affine model with constant n.

For natural rubber the affine model is of course successful in accounting for the SOS data, although the question of the intrinsic birefringence, and hence of the absolute magnitude of molecular orientation, must remain open. A close fit to high-strain data would be difficult to obtain with the two-component model: if one were to comment from the standpoint of this model alone, the discrepancy might well be ascribed to strain-induced crystallization.

At this stage, we should ask why the affine and two-component models should give different predictions of rubbery behaviour, for in one sense it might have been convenient if the two-component model were to have reduced to the affine for the rubbery case. We see the difference in the fact that the affine model deals with molecules isolated from their environments, and the only way in which a chain unit can be acted upon by an applied tensile stress is by the transmission of the stress along the unit's own chain: the behaviour of the unit is then directly linked to strain. In the two-component approach, a chain unit is considered as responding to its local stress field, which is transmitted by the environment of neighbouring chains as well as along the unit's own chain.

This point can be illustrated by considering the effect of stress on the unit A in the chain sketched in Fig. 34. If the chain is truly isolated, the effect of a tensile stress will initially be to rotate A away from the tensile axis, since it is rotation in this sense which can contribute to an increasing separation of the chain ends. In the two-component model, where the unit response is controlled by its local stress field, the tensile stress will have two

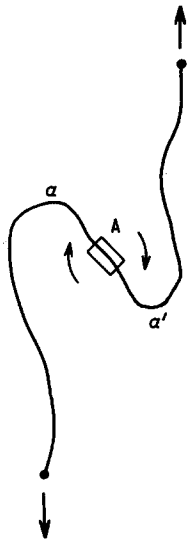

Figure 34 Illustration of the possible influence of the local stress field on a chain element "A". The consequent rotational alignment is in the opposite sense to that which result if the molecule were isolated and its end moved apart.

competing effects on A. It will tend to align it with the axis (the orientational component) and at the same time tend to rotate it in the other direction, thus eliminating the re-entrant loop from a to a'. In essence, then, the two-component model is particularly disfavouring the orientation of the unit normal to the tensile axis.

The most striking difference between the affine and two-component predictions concerns $\langle P_4 \rangle$. Plots of $\langle P_4 \rangle$ against stress (Fig. 15) and against strain (Fig. 16) for the two-component model show that this orientation parameter is slightly negative at low strains. In contrast, the affine model predicts low but positive values of $\langle P_4 \rangle$: the two models are compared in this respect in the plots of $\langle P_4 \rangle$ against $\langle P_2 \rangle$ of Fig. 27. The sign of $\langle P_4 \rangle$ at low strains should thus provide a distinctive test of one model against the other. However, the available $\langle P_4 \rangle$ data are tantalising on this point, for within the considerable scatter those for PVC and PET are if anything positive, while those for PMMA tend to be negative (it should perhaps be pointed out that any vestige of crystallinity would strongly bias $\langle P_4 \rangle$ to positive values). The issue of whether the two-component model is actually better at describing rubbery behaviour must thus remain open and await further and better data. We now move on to consider the influence of rate effects on each of the components in the model, in relation to deformation in the glassy state. This is done in Part 3.

Appendix I: The geometry of an ellipsoid of revolution

An ellipsoid of revolution is usually described by the equation

$$\frac{x^2}{a^2} + \frac{y^2}{a^2} + \frac{z^2}{l^2} = 1 \qquad \text{(A1)}$$

where a, l are the semiaxes and l is parallel to the axis of revolution z.

For our purposes we want to use coordinate axes parallel to those of a macroscopic body such as is shown by Fig. 35. Let these axes be u, v, w, with w vertical and u, v lying in our "sampling plane".

Consider a typical ellipsoidal unit with its z-axis at an angle ϕ to the specimen w-axis. We take y, v parallel and suppose ϕ to lie in the u–w plane (which is all right since we have cylindrical symmetry). With a suitable choice of origin it is possible to transform Equation A1 using the following transformation matrix:

$$\begin{vmatrix} \cos\phi & 0 & \sin\phi \\ 0 & 1 & 0 \\ -\sin\phi & 0 & \cos\phi \end{vmatrix} \begin{vmatrix} u \\ v \\ w \end{vmatrix} = \begin{vmatrix} x \\ y \\ z \end{vmatrix} \qquad \text{(A2)}$$

Equation A1 then becomes (abbreviating $\sin\phi = s$, $\cos\phi = c$):

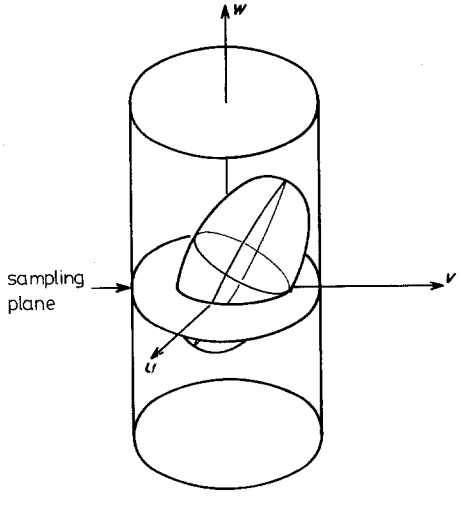

Figure 35 Coordinate axes of cylindrical body showing (enlarged) ellipsoidal unit.

$$\frac{u^2c^2 + w^2s^2 + 2uwsc}{a^2} + \frac{v^2}{a^2} + \frac{u^2s^2 + w^2c^2 - 2uwsc}{l^2} = 1 \qquad \text{(A3)}$$

Intercept with sampling plane

To calculate the area of our sampling plane we consider (Fig. 36) an ellipsoid whose axis makes an angle ϕ with the plane normal and whose centre lies a distance h from the plane. Such an ellipsoid will make an intercept of area A_i with the plane. We put $w = h$ in Equation A3 and after rearrangement obtain

$$u^2\left(\frac{c^2}{a^2} + \frac{s^2}{l^2}\right) + h^2\left(\frac{s^2}{a^2} + \frac{c^2}{l^2}\right) + \frac{v^2}{a^2} + 2uhsc\left(\frac{1}{a^2} - \frac{1}{l^2}\right) = 1 \qquad \text{(A4)}$$

This is still a bit clumsy, so we recall that the eccentricity e of an ellipsoid is defined by

$$a^2 = l^2(1 - e^2) \qquad \text{(A5)}$$

and that

$$\sin^2\phi + \cos^2\phi = 1$$

giving

$$\frac{u^2}{a^2}(1 - s^2e^2) + \frac{h^2}{a^2}(1 - c^2e^2) + \frac{v^2}{a^2} + 2\frac{uhsc}{a^2}e^2 = 1 \qquad \text{(A6)}$$

Substituting

$$u' = u + \frac{hsc \times e^2}{1 - (se)^2}$$

$$a' = \frac{a[1 - (se)^2 - (h/l)^2]^{1/2}}{[1 - (se)^2]}$$

$$b' = \frac{a[1 - (se)^2 - (h/l)^2]^{1/2}}{[1 - (se)^2]^{1/2}}$$

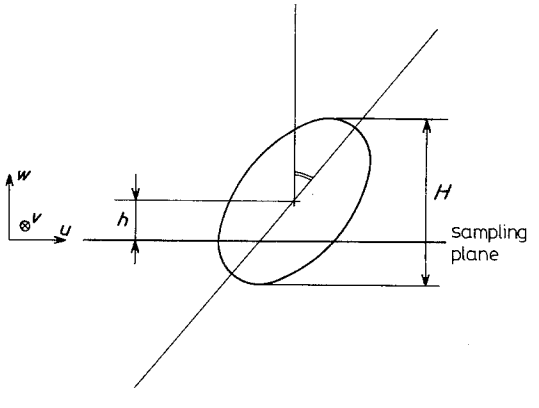

Figure 36 Cross-section through ellipsoidal unit and "sampling plane".

allows us to write Equation A6 in the form

$$\frac{u'^2}{a'^2} + \frac{v^2}{b'^2} = 1 \qquad \text{(A7)}$$

i.e., the intercept is itself elliptical, with area $\pi a'b'$, or

$$A_i = \frac{\pi a^2}{[1 - (se)^2]^{3/2}}[1 - (se)^2 - (h/l)^2] \qquad \text{(A8)}$$

We now make a convenient substitution:

$$Z^2 = 1 - (se)^2 \qquad \text{(A9)}$$

giving

$$A_i = \pi a^2 \frac{(Z^2 - (h/l)^2)}{Z^3} \qquad \text{(A10)}$$

Referring again to Fig. 36, it is easily shown (by putting $A_i = 0$ in Equation A10) that

$$H = 2lZ \qquad \text{(A11)}$$

The mean area of intercept $\langle A_i \rangle$ made by our ellipsoid within the "slice" of height H can then be found:

$$\langle A_i \rangle = \frac{\int A_i(h)\mathrm{d}h}{\int \mathrm{d}h} \qquad \text{with limits } h = -lZ, +lZ$$

$$= \frac{2\pi a^2}{3Z} \qquad \text{(A12)}$$

Energy argument

Consider the ellipsoid in Fig. 37. If the ellipsoid rotates by $\mathrm{d}\phi$, the applied stress σ (acting radially inwards) does work $\mathrm{d}W$, given by

$$\mathrm{d}W = \text{force} \times \text{distance}$$

$$= \sigma 2\pi RH\mathrm{d}R$$

$$= \sigma H\mathrm{d}A \qquad (\text{since } \mathrm{d}A = 2\pi R\mathrm{d}R)$$

$$= \frac{2lZ\sigma}{\alpha} \times \frac{\mathrm{d}\langle A_i \rangle}{\mathrm{d}Z} \times \mathrm{d}Z$$

$$= \frac{-2lZ\sigma}{\alpha} \times \frac{2}{3} \times \frac{\pi a^2}{Z^2} \times \mathrm{d}Z \qquad \text{(using Equation A12)}$$

$$= -V_e\sigma(1/Z)\mathrm{d}Z \qquad \text{(A13)}$$

where α is the packing density, and V_e is the volume per ellipsoid, given by

$$V_e = \frac{4\pi a^2 l}{3\alpha}$$

Hence, integrating from $Z = 1$ (i.e. $\phi = 0$) to some

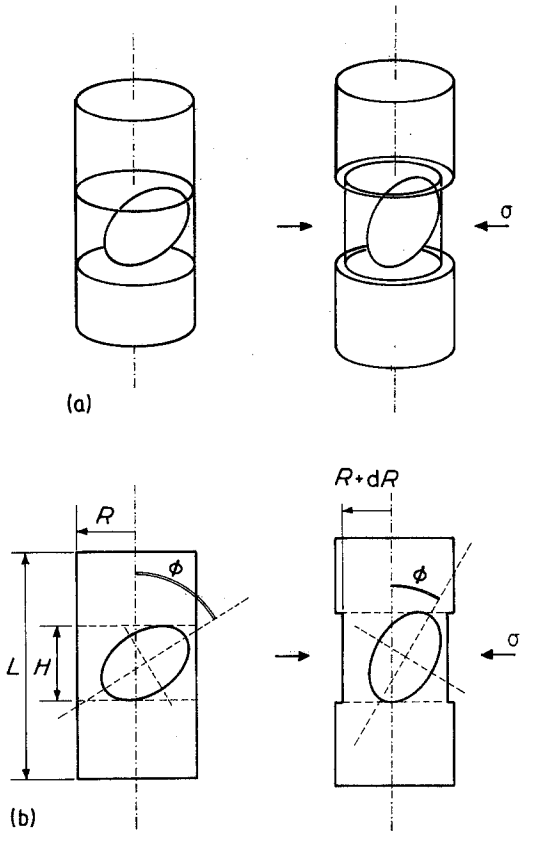

Figure 37 Orientational deformation: (a) three-dimensional (b) in cross-section.

general value of Z,

$$W = -V_e\sigma\ln(Z) \qquad \text{(A14)}$$

An argument analogous to our "first approximation" gives:

$$p'(Z)\mathrm{d}Z \sim D(Z) \times (2lZ/L) \times \exp(-W/kT) \times \mathrm{d}Z \qquad \text{(A15)}$$

We know the degeneracy $D(Z)$ in terms of ϕ:

$$D(\phi)\mathrm{d}\phi = \sin(\phi)\mathrm{d}\phi$$

but since

$$Z^2 = 1-(se)^2$$

we have

$$2Z\frac{\mathrm{d}Z}{\mathrm{d}\phi} = -2sce^2$$

and also

$$c^2 = 1-s^2 = (1/e)[Z^2-(1-e^2)] \qquad \text{(A16)}$$

Hence

$$\begin{aligned} D(Z)\mathrm{d}Z &= s\mathrm{d}Z(\mathrm{d}\phi/\mathrm{d}Z) \\ &= \frac{-sZ\mathrm{d}Z}{sce^2} \\ &= \frac{Z\mathrm{d}Z}{e[Z^2-(1-e^2)]^{1/2}} \end{aligned} \qquad \text{(A17)}$$

[taking the negative root to give a positive $D(Z)$]. Also

$$\exp(-W/kT) = \exp[(V_e\sigma/kT)\ln(Z)] = Z^q \qquad \text{(A18)}$$

where

$$q = V_e\sigma/kT$$

Hence

$$p'(Z)\mathrm{d}Z \sim \frac{2lZ}{\lambda} \times \frac{1}{e} \times \frac{ZZ^q\mathrm{d}Z}{[Z^2-(1-e^2)]^{1/2}} \qquad \text{(A19)}$$

We make a further useful substitution

$$\psi = \arccos(m/Z) \qquad \text{(A20)}$$

where $m^2 = (1-e^2)$, so that

$$\mathrm{d}Z = (Z^2/m)\sin\psi\,\mathrm{d}\psi = m\sin\psi\sec^2\psi\,\mathrm{d}\psi$$

and

$$\sin\psi = (1/Z)[Z^2-(1-e^2)]^{1/2}$$

Equation A19 can now be written as:

$$p'(\psi)\mathrm{d}\psi \sim \frac{2l}{\lambda} \times \frac{1}{em}(m\sec\psi)^{q+3}\mathrm{d}\psi \qquad \text{(A21)}$$

Extension ratio

The total area of a cross-section through our assemblage, intersected by N units, is now given by

$$\frac{A}{N} = \frac{\int A_i(Z)p'(Z)\mathrm{d}Z}{\alpha\int p'(Z)\mathrm{d}Z} \qquad \text{(A22)}$$

with limits $\phi = 0$, $Z = 1$
and $\phi = \pi/2$, $Z = (1-e^2)^{1/2}$

$$= \tfrac{2}{3}\pi l^2(1-e^2)\frac{\int(1/Z)p'(Z)\mathrm{d}Z}{\alpha\int p'(Z)\mathrm{d}Z} \qquad \text{(A23)}$$

$$= \tfrac{2}{3}\pi a^2\frac{1}{\alpha m}\frac{\int\sec^{q+2}\psi\,\mathrm{d}\psi}{\int\sec^{q+3}\psi\,\mathrm{d}\psi} \qquad \text{(A24)}$$

with limits $\psi = \arccos m$,
$\psi = \arccos 1 = 0$.

This is easily evaluated numerically, but when $q = 0$ we can use two standard integrals

$$\int\sec^n x\,\mathrm{d}x = \frac{1}{n-1} \times \frac{\sin x}{\cos^{n-1}x} + \frac{n-2}{n-1}\int\sec^{n-2}x\,\mathrm{d}x \qquad \text{(A25)}$$

$$\int\sec x\,\mathrm{d}x = \ln(\sec x + \tan x) \qquad \text{(A26)}$$

to give the following expression for the initial area A_0:

$$\frac{A_0}{N_0} = \frac{1}{3} \times \frac{\pi a^2}{\alpha m} \times \frac{(\tan \psi)}{(\sin \psi / \cos^2 \psi) + \int \sec \psi \, d\psi}$$

$$= \frac{1}{3} \times \frac{\pi a^2}{\alpha m} \times \frac{(1/m)(1-m^2)^{1/2}}{[(1-m^2)^{1/2}/m^2] + \ln \{[1+(1-m^2)^{1/2}]/m\}}$$

$$= \frac{4}{3\alpha} \pi a^2 \left[1 + \frac{m^2}{e} \ln \left(\frac{1+e}{m}\right)\right]^{-2} \quad \text{(A27)}$$

Hence, if $N = N_0$:

$$\frac{A_0}{A} = \frac{2m}{\{1 + (m^2/e) \ln [(1+e)/m]\}} \times \frac{\int \sec^{q+3} \psi \, d\psi}{\int \sec^{q+2} \psi \, d\psi} \quad \text{(A28)}$$

This is an expression for the orientational component λ_0 of the extension ratio. Its maximum is found by letting q tend to infinity, so that $\phi = 0$ for all units:

$$\lambda_0^{\max} = 2\left[1 + \frac{m^2}{e} \ln \left(\frac{1+e}{m}\right)\right]^{-1} \quad \text{(A29)}$$

Orientation functions

To obtain the Legendre polynomials P_{2n} we have to evaluate integrals such as

$$\langle \cos^2 \phi \rangle = \frac{\int \cos^2 \phi p(\phi) d\phi}{\int p(\phi) d\phi} \quad \text{(A30)}$$

where, if W is the energy associated with a unit at angle ϕ,

$$p(\phi)d\phi \sim D(\phi) \exp(-W/kT) d\phi \quad \text{(A31)}$$

We again work in terms of the variable Z; we substitute for $p(\phi)d\phi$ using Equations A17 and A18, and for $\cos^2 \phi$ using Equation A16. Then:

$$p(Z)dZ \sim \frac{1}{e} \times \frac{-ZZ^q dZ}{[Z^2 - (1-e^2)]^{1/2}}$$

$$= \frac{-m^{q+1}}{e} \sec^{q+2} \psi \, d\psi \quad \text{(A32)}$$

and

$$\cos^2 \phi = \frac{1}{e}[Z^2 - (1-e^2)] = \frac{1-e^2}{e^2}(\sec^2 \psi - 1) \quad \text{(A33)}$$

If we abbreviate $\int \sec^{q+n} \psi \, d\psi = I_n$, Equation A30 simplifies to

$$\langle \cos^2 \phi \rangle = \frac{m^2}{e^2} \times \frac{I_4 - I_2}{I_2} \quad \text{(A34)}$$

from which $\langle P_2(\cos \phi) \rangle$ may easily be found. By a similar method:

$$\langle \cos^4 \phi \rangle = \frac{m^4}{e^4} \times \frac{I_6 - 2I_4 + I_2}{I_2} \quad \text{(A35)}$$

and so on for as many $\langle P_{2n} \rangle$ as we require.

Appendix II: The constraint concept and cross-linking

We can compare the "constraint" idea introduced above with the molecular cross-linking by the following argument, if we assume that the fractional constraint is primarily to be associated with interchain cross-linking. Consider an assemblage of chains connected by chemical and/or mechanical cross-links, with a "chain segment" defined as the section of a molecule between two such cross-links. Let the number of chain segments per unit volume be N_s, and neglect chain ends. If the cross-links are tetrafunctional (the meeting point of four chain segments), their number per unit volume will be $N_s/2$, and the mean volume per cross-link $2/N_s$: we can imagine each link being surrounded by a local 'cross-link region" of mean volume $2/N_s$.

Assume that at zero strain the segments are randomly oriented: a "slice" of area A_0 through the assemblage will then, on average, cut through a number of "cross-link regions" given by

$$\frac{A_0}{(2/N_s)^{2/3}}$$

Now suppose we go to maximum extensional strain. If we take the stress to be uniaxial and the deformation affine, the number of "cross-link regions" cut by our slice will remain the same. But

the number of chains cut – or the number of "units" intersecting the sampling plane – will at maximum extensional strain be simply N^*. Remembering that there are twice as many chain segments as crosslinks, we can write

$$N^* = \frac{2A_0}{(2/N_s)^{2/3}} \quad \text{(B1)}$$

We can also put $N^* = A/A_c$, where A is the area of the sampling plane and A_c is defined as the mean cross-sectional area per chain cut (which will depend, of course, on the orientational component of strain). Hence

$$\frac{A_0}{A} = \frac{(2/N_s)^{2/3}}{2A_c} \quad \text{(B2)}$$

The corresponding expression given by our model at maximum extensional strain is simply

$$\frac{A_0}{A} = \frac{N_0}{N^*}\lambda_0 = K\lambda_0 = K\frac{A_{c0}}{A_c} \quad \text{(B3)}$$

where A_{c0} is the value of A_c at zero strain. Hence, equating the two expressions

$$K = \frac{(2/N_s)^{2/3}}{2A_{c0}} \quad \text{(B4)}$$

so that the cross-link density $N_s/2$ will be proportional to $(K)^{3/2}$, with the constant of proportionality $(2A_{c0})^{-3/2}$ easily accessible from a knowledge of chain cross-section and packing density.

For the first approximation model, A_{c0} is simply twice the chain cross-section divided by packing density; if we take a value of 0.20 nm^2 for A_{c0} and assume a packing density of 0.5, then the constant of proportionality becomes about 5×10^{28}. Taking $K = 3$ then gives a cross-link density of approximation 10^{28} m^{-3}, which is about the same as the Gaussian theory suggests for a rubber with an initial modulus (in uniaxial tension) of 2.5 MPa at 300 K. This would correspond to a rather highly cross-linked network.

References

1. D. J. BROWN and A. H. WINDLE, *J. Mater. Sci.* 19 (1984) 1997.
2. R. LOVELL, G. R. MITCHELL and A. H. WINDLE, *Discuss. Faraday Soc.* 68 (1980) 46.
3. R. LOVELL and A. H. WINDLE, *Polymer* **22** (1981) 175.
4. M. KASHIWAGI, M. J. FOLKES and I. M. WARD, *ibid.* **12** (1971) 697.
5. D. J. BROWN and G. R. MITCHELL, *J. Polym. Sci., Polym. Lett. Ed.* **21** (1983) 341.
6. G. R. MITCHELL, M. PICK and A. H. WINDLE, *Polym. Commun.* **24** (1983) 16.
7. A. CUNNINGHAM, I. M. WARD, H. A. WILLIS and V. ZICHY, *Polymer* **15** (1974) 749.
8. J. H. NOBBS, D. I. BOWER, I. M. WARD and D. PATTERSON, *ibid.* **15** (1974) 287.
9. J. H. NOBBS, D. I. BOWER and I. M. WARD, *ibid.* **17** (1976) 25.
10. J. PURVIS and D. I. BOWER, *J. Polym. Sci., Polym. Phys. Ed.* **14** (1976) 1461.
11. F. RIETSCH, R. A. DUCKETT and I. M. WARD, *Polymer* **20** (1979) 1133.
12. J. S. FOOT and I. M. WARD, *J. Mater. Sci.* **10** (1975) 955.
13. D. J. BROWN, to be published.
14. M. PICK, PhD thesis, University of Cambridge (1979).
15. M. PICK, R. LOVELL and A. H. WINDLE, *Polymer* **21** (1980) 10171.
16. S. HIBI, M. MAEDA, H. KUBOTA and T. MIURA, *ibid.* **18** (1977) 137.
17. M. E. R. ROBINSON, D. I. BOWER and W. F. MADDAMS, *J. Polym. Sci., Polym. Phys. Ed.* **16** (1978) 2115.
18. Y. SHINDO, B. E. READ and R. S. STEIN, *Makromol. Chem.* **118** (1968) 272.
19. J. G. RIDER and E. HARGREEVES, *J. Phys. D.* **3** (1970) 993.
20. L. R. G. TRELOAR, *Trans. Faraday Soc.* **40** (1944) 59.
21. S. M. GUMBRELL, L. MULLINS and R. S. RIVLIN, *Trans. Faraday Soc.* **49** (1953) 1495.
22. L. MULLINS, *J. Polym. Sci.* **19** (1956) 225.
23. K. J. SMITH, A. GREENE and A. CIFERRI, *Kolloid Z.* **194** (1964) 49.
24. M. C. MORRIS, *J. Appl. Polym. Sci.* 8 (1964) 545.
25. J. A. C. HARWOOD, L. MULLINS and A. R. PAYNE, *ibid.* **9** (1965) 3011.
26. K. J. SMITH and D. PUETT, *J. Appl. Phys.* **37** (1966) 346.
27. R. J. MORGAN and L. R. G. TRELOAR, *J. Polym. Sci., Part A2* **10** (1972) 51.
28. L. R. G. TRELOAR, *Trans. Faraday Soc.* **43** (1947) 277, 284.
29. Y. SHINDO and R. S. STEIN, *J. Polym. Sci., Part A2* 7 (1969) 2115.
30. W. O. S. DOHERTY, K. L. LEE and L. R. G. TRELOAR, *Brit Polym. J.* **12** (1980) 19.
31. L. R. G. TRELOAR and G. RIDING, *Proc. Roy. Soc. London* **A369** (1979) 261.
32. *Idem, ibid.* (1979) 281.
33. J. H. NOBBS and D. I. BOWER, *Polymer* **19** (1978) 1100.
34. Part 3 of this series of papers.
35. M. KASHIWAGI and I. M. WARD, *Polymer* **13** (1972) 145.
36. J. H. DUMBLETON, *J. Polym. Sci., Part A2* **6** (1968) 795.
37. D. B. CAVANAUGH and C. H. WANG, *J. Polym. Sci., Polym. Phys. Ed.* **19** (1981) 1911.
38. J. PURVIS and D. I. BOWER, *Polymer* **15** (1974) 645.
39. N. I. SHISHKIN and M. F. MILAGIN, *Sov. Phys. Solid State* 4 (1963) 1967.

Received 7 September
and accepted 22 September 1983